Title

Secreted Effector Proteins of Poplar Leaf Spot and Stem Canker Pathogen Sphaerulina musiva Manipulate Plant Immunity and Contribute to Virulence in Diverse Ways.

Journal

Molecular Plant-Microbe Interactions, 36(12)

ISSN

0894-0282

Authors

Zhao, Yao

Zheng, Xinyue

Tabima, Javier F

et al.

Publication Date

2023-12-01

DOI

10.1094/mpmi-07-23-0091-r

MPMI Vol. 36, No. 12, 2023, pp. 779–795, https://doi.org/10.1094/MPMI-07-23-0091-R

Secreted Effector Proteins of Poplar Leaf Spot and Stem Canker Pathogen *Sphaerulina musiva* Manipulate Plant Immunity and Contribute to Virulence in Diverse Ways

Yao Zhao,[2] Xinyue Zheng,[1] Javier F. Tabima,[3,4] Sheng Zhu,[1] Kelsey L. Søndreli,[3] Hope Hundley,[5] Diane Bauer,[5] Kerrie Barry,[5] Yaxin Zhang,[1] Jeremy Schmutz,[6] Yuanchao Wang,[2] Jared M. LeBoldus,[3,7,†] and Qin Xiong[1,†]

[1] Co-Innovation Center for Sustainable Forestry in Southern China, College of Biology and the Environment, Nanjing Forestry University, Nanjing 210095, China
[2] Department of Plant Pathology, Nanjing Agricultural University, Nanjing 210095, China
[3] Department of Botany and Plant Pathology, College of Agricultural Sciences, Oregon State University, Corvallis, OR 97331, U.S.A.
[4] Department of Biology, Clark University, Worcester, MA 01610, U.S.A.
[5] U.S. Department of Energy Joint Genome Institute, Lawrence Berkeley National Laboratory, Berkeley, CA 94720, U.S.A.
[6] HudsonAlpha Institute for Biotechnology, Huntsville, AL 35806, U.S.A.
[7] Department of Forest Engineering, Resources and Management, College of Forestry, Oregon State University, Corvallis, OR 97331, U.S.A.

Accepted for publication 4 August 2023.

Fungal effectors play critical roles in manipulating plant immune responses and promoting colonization. *Sphaerulina musiva* is a heterothallic ascomycete fungus that causes Septoria leaf spot and stem canker disease in poplar (*Populus* spp.) plantations. This disease can result in premature defoliation, branch and stem breakage, increased mortality, and plantation failure. However, little is known about the interaction between *S. musiva* and poplar. Previous work predicted 142 candidate secreted effector proteins in *S. musiva* (SmCSEPs), 19 of which were selected for further functional characterization in this study. SmCSEP3 induced plant cell death in *Nicotiana benthamiana*, while 8 out of 19 tested SmCSEPs suppressed cell death. The signal peptides of these eight SmCSEPs exhibited secretory activity in a yeast signal sequence trap assay. Confocal microscopy revealed that four of these eight SmCSEPs target both the cytoplasm and the nucleus, whereas four predominantly localize to discrete punctate structures. Pathogen challenge assays in *N. benthamiana* demonstrated that the transient expression of six SmCSEPs promoted *Fusarium proliferatum* infection. The expression of these six *SmCSEP* genes were induced during infection. SmCSEP2, SmCSEP13, and SmCSEP25 suppressed chitin-triggered reactive oxygen species burst and callose deposition in *N. benthamiana*. The candidate secreted effector proteins of *S. musiva* target multiple compartments in the plant cell and modulate different pattern-triggered immunity pathways.

Keywords: candidate secreted effector proteins (CSEPs), plant immunity, poplar, prediction, *Sphaerulina musiva*, subcellular localization, virulence

[†]Corresponding authors: Q. Xiong; xiongqin@njfu.edu.cn, and J. M. LeBoldus; jared.leboldus@science.oregonstate.edu

Y. Zhao and X. Zheng contributed equally to this work and share first authorship.

Author contributions: Q.X., Y.Z., and X.Y.Z conceived and designed the experiments. Y.Z., X.Y.Z., K.L.S., Y.X.Z., and Q.X. performed the experiments. Q.X., Y.Z., X.Y.Z., J.F.T., and S.Z. analyzed the experimental data. H.H., D.B., K.B., Y.C.W., and J.M.L. contributed reagents/materials/analysis tools. Y.Z., Q.X., and J.M.L. wrote the paper. All authors read and approved the final manuscript.

Funding: This work was supported, in part, by grants provided to Q. Xiong by the National Natural Science Foundation of China (31600512), China Postdoctoral Science Foundation (2021M691605), Postdoctoral Science Foundation of Jiangsu Province (2021K641C), China Scholarship Council (201908320031), and the Priority Academic Development Program of Jiangsu Higher Education Institutions. This study was also supported by Department of Energy (DOE) Office of Science, Office of Biological and Environmental Research grant DE-SC0018196 and U.S. Department of Agriculture grant 2012-34103-19771 (to J. M. LeBoldus). The work (proposal: 10.46936/10.25585/60000891) conducted by the U.S. Department of Energy Joint Genome Institute (https://ror.org/04xm1d337), a DOE Office of Science User Facility, is supported by the Office of Science of the U.S. Department of Energy operated under contract no. DE-AC02-05CH11231.

***e*-Xtra:** Supplementary material is available online.

The author(s) declare no conflict of interest.

Poplar, a widely cultivated fast-growing tree species, is a valuable commercial resource for the manufacture of pulp, paper, timber, and other wood-based products, in addition to being a potential bioenergy feedstock (Polle et al. 2013; Sannigrahi et al. 2010). However, the fungal pathogen *Sphaerulina musiva* (Peck) Quaedvlieg, Verkley & Crous (syn. = *Septoria musiva*) infects multiple poplar species and their hybrids in North America, causing severe leaf spot and stem canker disease (Feau et al. 2010; Lenz et al. 2021). Septoria leaf spot causes premature defoliation, reducing photosynthetic area and resulting in yield losses. Septoria stem canker can girdle and weaken branches

and stems, increasing the risk of stem breakage or premature crown death (Feau et al. 2010; Ostry and McNabb 1985). In susceptible poplar species and hybrids, the incidence of Septoria stem canker can reach 100%, often leading to plantation failure (Dunnell et al. 2016; Feau et al. 2010; Ostry et al. 1989). Furthermore, the host range of *S. musiva* has expanded with reports from *Salix lucida* (Feau and Bernier 2004). The distribution of the pathogen continues to expand in North America (Søndreli et al. 2020) and around the world (Ares and Gutierrez 1996; Dos Santos et al. 2010; Feau et al. 2010; Jeger et al. 2018). The European and Mediterranean Plant Protection Organization has classified *S. musiva* as a regulated quarantine pathogen because of its invasiveness (Jeger et al. 2018; Niemczyk and Thomas 2020). Septoria leaf spot and stem canker is a major economic and ecological threat to poplar-producing regions worldwide. Currently, the most effective strategy to manage this disease is to plant resistant genotypes, which requires a greater understanding of both the genetics of disease resistance and interactions between *S. musiva* and poplar.

Pathogen–plant interactions are intricate and dynamic, and plants possess two levels of innate immunity in response to pathogen infection (Chisholm et al. 2006; Jones and Dangl 2006). Pathogen-associated molecular pattern-triggered immunity (PTI) is the first level of plant immunity, which is sufficient to detect and ward off most potential pathogenic microbes. This is often called non-host resistance (Dodds and Rathjen 2010). PTI is triggered by conserved pathogen/microbe-associated molecular patterns (PAMPs or MAMPs) that are perceived by plant pattern-recognition receptors (Boller and Felix 2009; Jones and Dangl 2006). The activation of PTI signaling results in rapid responses that include the production of reactive oxygen species (ROS), cytosolic calcium bursts, callose deposition, mitogen-activated protein kinase pathway activation, and defense-related gene expression (Lo Presti et al. 2015; Stael et al. 2015). To circumvent and overcome PTI, the adapted pathogen secretes and delivers a variety of so-called effectors into the plant cytoplasm or apoplastic space for successful infection (de Jonge et al. 2011; Stergiopoulos and de Wit 2009; Zhang et al. 2014). In turn, plants deploy their second layer of immunity, called effector-triggered immunity (ETI), to recognize pathogen effectors via corresponding resistance (R) proteins. ETI activates a higher-amplitude defense than PTI and typically manifests as localized cell death, termed the hypersensitive response (HR) (Dodds and Rathjen 2010). Understanding how *S. musiva* effector proteins suppress host resistance can elucidate molecular mechanisms of pathogenicity and contribute to breeding efforts developing durable resistance to Septoria leaf spot and stem canker disease in poplar. To date, no *S. musiva* effectors have been functionally characterized.

During infection, effectors secreted by filamentous plant pathogens serve a crucial function in the plant–pathogen interface (Selin et al. 2016). Recent advances in "omics" and bioinformatics have led to the rapid discovery of numerous candidate secreted effector proteins (CSEPs) that can be targeted for functional validation. This can be challenging because of a lack of conserved sequence features common to fungal effectors. In addition, the small number of identified and validated fungal effectors for many species limits the effectiveness of comparative approaches (Sperschneider et al. 2015). In contrast to bacterial and oomycete effectors, relatively few fungal effectors in pathogens of forest trees have been characterized (Ahmed et al. 2018; de Guillen et al. 2019; Dos Santos et al. 2021; Rahman et al. 2021). Typically, effectors are selected for functional analysis using the following criteria: a predicted secretion signal, small size, cysteine-rich, differentially expressed during in planta infection, and lacking a transmembrane domain (Lo Presti et al. 2015; Sperschneider et al. 2015). We used these criteria to select *S. musiva* effectors for further characterization.

Genome analyses highlighted a total of 142 *CSEP* genes from the *S. musiva* reference genome using SignalP 3.0 and EffectorP 2.0 (Tabima et al. 2020). Next-generation sequencing technologies have also provided access to gene expression profiles during poplar infection by *S. musiva*, for example, a comparative expression analysis between resistant (DN34 and NM6) and susceptible (DN164 and NC11505) poplar clones inoculated with *S. musiva* by RNA sequencing (RNA-Seq) analysis (Liang et al. 2014). Muchero et al. (2018) employed multifaceted analyses, such as genome-wide association studies and transcriptomics to identify resistance- or susceptibility-associated loci in *Populus trichocarpa* (BESC-22 and BESC-801, respectively) inoculated with *S. musiva*. Moreover, Foster et al. (2015) also performed a transcriptomic analysis of three poplar species (*Populus deltoides*, *Populus balsamifera*, and *Populus tremuloides*) during leaf infection by their naturally coevolved *Sphaerulina* pathogens (*S. musiva*, *Sphaerulina populicola*, and a new undescribed species, Ston1). This work all focused on the host response, neglecting to dissect pathogenesis-associated gene expression patterns in *S. musiva*. Thus, we combined a comparative genomics approach (Tabima et al. 2020) with transcriptomics to better focus functional characterization efforts in the *S. musiva*–poplar interaction.

Functional characterization of effectors through in vitro or heterologous systems has been widely reported in the literature. For example, a high-throughput screen of 169 predicted RXLR effectors in *Phytophthora sojae*, using transient expression in tobacco leaves, revealed that 23 could suppress the programmed cell death (PCD) triggered in *Nicotiana benthamiana* leaves, and 11 could trigger cell death, chlorosis, or mottling (Ma et al. 2015; Wang et al. 2011). In the rice blast pathogen *Pyricularia oryzae*, five candidate effectors suppressed the BAX-triggered PCD (BT-PCD) in tobacco leaves, facilitating fungal propagation and pathogenicity (Dong et al. 2015). An additional five induced cell death in both host (rice) and the non-host (tobacco) plants (Chen et al. 2013), and eight induced cell death in tobacco leaves only (Guo et al. 2019). Exogenous treatment of rice seedlings with recombinant effectors resulted in enhanced resistance to *P. oryzae* (Guo et al. 2019). In another example, the VmHEP1 effector from the woody plant pathogen *Valsa mali* suppressed BT-PCD in *N. benthamiana*, and the double deletion of *VmHEP1* and *VmHEP2* reduced *V. mali* virulence in apples (Zhang et al. 2019). As a result, *Agrobacterium*-mediated infiltration of tobacco (*N. benthamiana*) was used as a heterologous system to test the effect of the selected SmCSEPs, on several well-characterized plant immunity pathways, including HR-induced cell death, suppression of the PCD pathway, ROS accumulation, and leakage of essential electrolytes.

In vitro or heterologous approaches are also used to study the site of activity of fungal effectors. These studies have revealed that once secreted by pathogens, two classes of effectors have been observed. Apoplastic effectors reside in the extracellular matrix (Rocafort et al. 2020; Wang et al. 2019), whereas cytoplasmic effectors are translocated into the plant cell, targeting specific organelles or structures (Figueroa et al. 2021). Characterized plant pathogen effectors have been demonstrated to be extremely versatile, targeting diverse plant compartments and elements of the plant immune system to promote infection. Thus, localization of effectors can provide important clues to their functions and/or mode of action.

In the present study, we selected 19 SmCSEPs, using their expression profiles in a dual RNA-Seq experiment. In this experiment, three susceptible poplar genotypes sampled across several time points were used to select candidate effectors for functional characterization. Initially, we investigated their ability

to induce HR or suppress BAX- and INF1-triggered PCD via *Agrobacterium*-mediated transient expression. We employed a yeast signal sequence trap (YSST) assay to verify the secretory activity of their predicted signal peptides (SPs) and used fluorescence microscopy and fluorescent tags to predict their subcellular localization in planta. We then tested the ability of select effectors, overexpressed in *N. benthamiana*, to enhance susceptibility to *Fusarium proliferatum* by suppressing PTI-induced HR triggered by INF1 and BAX. The expression of these effectors during *S. musiva* infection on poplar leaves was monitored by real-time PCR. In addition, suppression of ROS and callose deposition triggered by chitin were also evaluated. To our knowledge, this is the first study to identify and functionally characterize effector proteins from the poplar pathogen *S. musiva*.

Results

Selection of candidate effector proteins secreted by *S. musiva*

Based on previous work, a total of 142 SmCSEPs were predicted using the *S. musiva* SO2202 v.1.0 reference genome and the SignalP 3.0/SignalP 5.0 (D score > 0.8) and EffectorP2.0 (P value > 0.5) software packages (Tabima et al. 2020). To date, the majority of all described effectors are upregulated during host colonization. As a result, to reduce the number of effector candidates, we prioritized the in planta-expressed CSEPs following the initial bioinformatic predictions. Thus, we examined the temporal expression patterns of 142 *SmCSEP* genes during infection using RNA-Seq. We inoculated three susceptible poplar genotypes (BESC367, BESC347, and GW9807) with *S. musiva* isolate MN-14 and monitored the temporal pattern of gene expression at 24 and 72 h postinoculation (hpi). At both time points, approximately the same percentage of RNA-Seq reads mapped to the *S. musiva* reference genome. All comparisons were made relative to the mock-inoculated controls. This was less than 20% of total reads. Analysis of the fungal reads identified 43 *SmCSEP* genes at 24 hpi and 48 *SmCSEP* genes at 72 hpi that were highly expressed in the inoculated trees relative to the controls. Across both time points and all three susceptible genotypes, 28 *SmCSEPs* with the greatest number of transcripts were selected for functional characterization (Fig. 1; Supplementary Table S1).

Bioinformatic prediction of proteinaceous effectors

A total of 28 *SmCSEP* genes were successfully cloned from the cDNA of poplar inoculated with *S. musiva* isolate MN-14 and

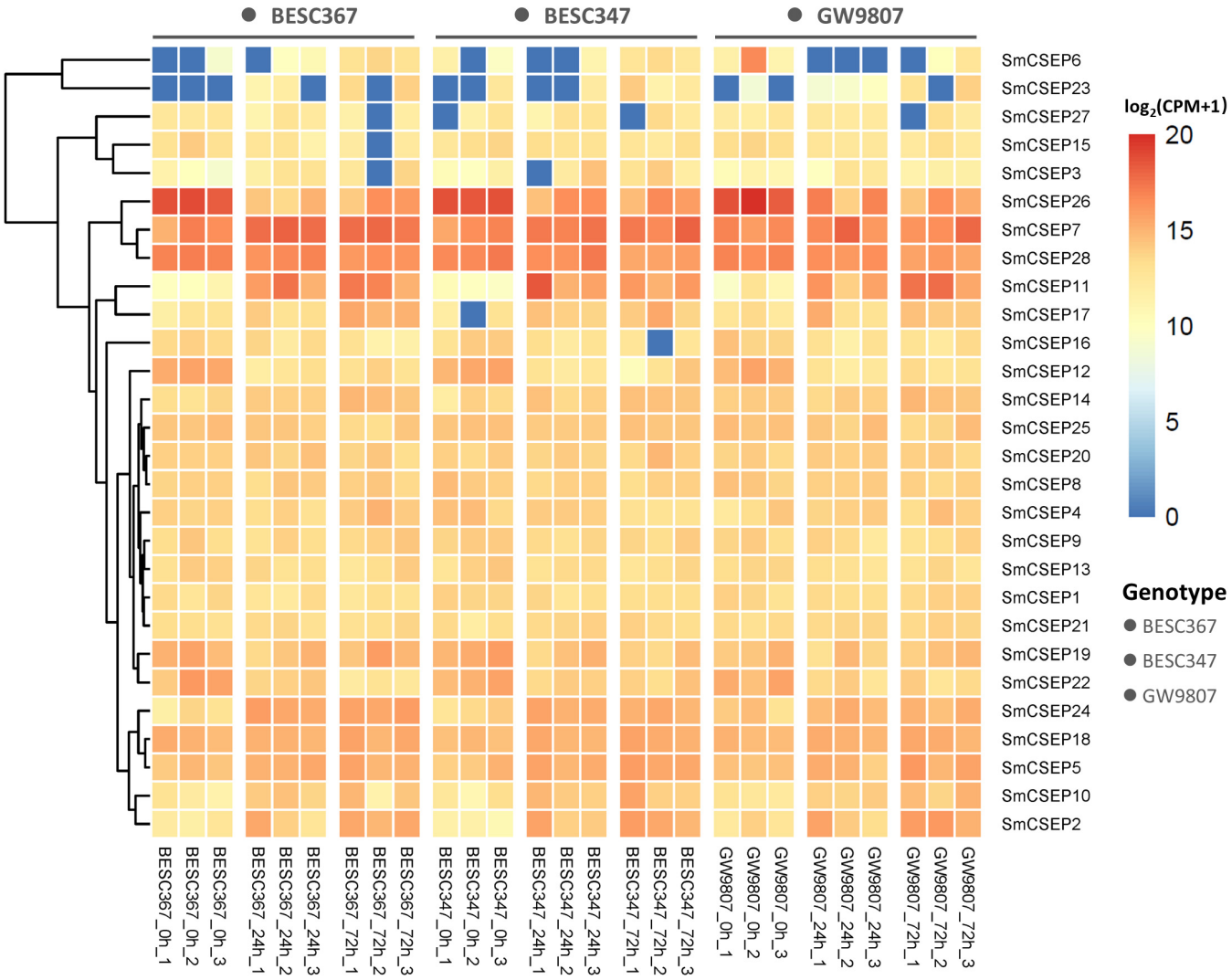

Fig. 1. Heat map of expression level of 28 selected *SmCSEP*s during compatible interactions with three susceptible poplar genotypes. The first three columns are poplar genotype BESC367 inoculated with *Sphaerulina musiva* MN-14 at 0, 24, and 72 h; the second three columns are poplar genotype BESC347 inoculated with *S. musiva* MN-14 at 0, 24, and 72 h; the last three columns are poplar genotype GW9807 inoculated with *S. musiva* MN-14 at 0, 24, and 72 h. The gene expression level from each time point was calculated by $\log_2(\text{CPM} + 1)$ (CPM, read counts per million) for heat-map visualization. The heat map was visualized using the R package pheatmap (v1.0.12, https://cran.r-project.org/web/packages/pheatmap/index.html).

then sequenced. The genomic features, potential function, amino acid sequences, and molecular weight of these 28 SmCSEPs are listed in Supplementary Table S3. The amino acid sequences of half ($n = 14$) the SmCSEPs were identical to the reference. However, 13 cloned SmCSEPs had several single or missense mutations, and one had a short insertion (Supplementary Table S3). To improve the efficiency and accuracy of the SmCSEPs selection, multiple prediction approaches were used. Neither the SignalP 5.0 nor the TargetP 2.0 prediction analyses revealed any SP sequence in SmCSEP11, SmCSEP15, SmCSEP17, or SmCSEP19 (Supplementary Table S4, bold). These were subsequently excluded from the list of effector candidates. To further rule out proteins likely to be retained in the plasma membrane, the remaining 24 SmCSEPs were subjected to transmembrane domain (TMD) prediction by the TMHMM tool (Krogh et al. 2001). SmCSEP21 contained two TMDs and seven of the other SmCSEPs contained one TMD (Supplementary Table S4, italic). Of these seven SmCSEPs, three SmCSEPs (SmCSEP4, SmCSEP5, and SmCSEP13) with predicted TMDs also had SPs (Supplementary Table S4, italic and underscore) and were not excluded. In total, the final number of SmCSEPs selected for further functional analysis in *S. musiva*–plant interactions was 19.

BLAST homology searches against publicly available sequence databases at the NCBI revealed that 13 out of 19 SmCSEPs are hypothetical or uncharacterized proteins, while the remaining six SmCSEPs show conserved protein domains or similarity to characterized proteins (Supplementary Table S3), some of which have been reported to be associated with pathogenesis in other fungal pathogens.

Certain SmCSEPs suppress PCD induced by BAX and PAMP-INF1 in *N. benthamiana*

To assess whether the 19 selected SmCSEPs regulate plant innate immunity, BAX-triggered PCD suppression in *N. benthamiana* via an *Agrobacterium*-mediated transient expression assay was performed. A total of 19 *SmCSEP* genes were successfully cloned from the cDNA of *S. musiva* isolate MN-14 and then subcloned into the *Potato virus X* (PVX) vector pGR107. BAX, a pro-apoptotic Bcl-2 protein found in mice, triggers defense-related HR in a variety of plant species (Lam et al. 2001; Oltval et al. 1993). BAX was coexpressed with each of the SmCSEPs in *N. benthamiana* leaves (Fig. 2, injection site no. 4). Only sites infiltrated with buffer (Fig. 2, injection site no. 3) or the *Agrobacterium* suspension carrying a pGR107-green fluorescent protein (GFP) vector (Fig. 2, injection site no. 2) did not result in PCD, whereas sites infiltrated with GFP (No. 5) or Buffer (No. 6) and then challenged with BAX 24 h later exhibited pronounced cell death, indicating that PCD was successfully induced by BAX.

The *Agrobacterium* suspensions carrying only the tested SmCSEPs (Fig. 2, injection site no. 1) did not cause PCD, except SmCSEP3. The SmCSEP3 itself induced clear necrosis (red circle line) at 2 days postinjection (dpi) (Fig. 2; Supplementary Fig. S1). Following a similar challenge with BAX, 7 out of the 19 tested SmCSEPs completely suppressed BT-PCD infiltration site No. 4, while SmCSEP6 partially suppressed BT-PCD (Fig. 2). The remaining 11 had no obvious effect.

To further confirm the suppression effect of the tested SmCSEPs on PCD, we also tested the effect of SmCSEPs on the suppression of PCD induced by INF1, a *Phytophthora infestans* extracellular elicitin that acts as a PAMP inducing HR (Kamoun et al. 1997). The transient expression of INF1 in tobacco leaves through *Agrobacterium* infiltration triggered significant PCD, and all 19 effectors exhibited the same cell death activity when challenged with INF1-mediated PCD as that observed with BT-PCD (Fig. 2). In summary, 8 of the 19 tested SmCSEPs suppress PCD both at the PAMP-induced level (INF1) and through mitochondrial PCD (BAX).

Secretion validation of the SmCSEP SPs

SignalP software predicted that all eight SmCSEPs contain SPs at the N-terminus, suggesting that these proteins are secreted. To test this, a YSST assay was used (Yin et al. 2021). Each predicted SP-encoding sequence of the eight SmCSEPs was successfully fused in frame with a truncated *SUC2* gene that encodes invertase (without its native SP) in the pSUC2 vector and then transformed into the invertase secretion-deficient YTK12 strain. The non-transformed YTK12 strain, which lacks the sucrose invertase gene, failed to grow in the CMD-W medium (containing sucrose and glucose, but not tryptophan) (Fig. 3). Yeast transformants harboring an pSUC2 EV, which were used as a negative control, grew on the CMD-W medium (yeast growth without invertase secretion), but not in the YPRAA medium (yeast growth only when invertase is secreted) containing raffinose only (Fig. 3). By contrast, strains carrying pSUC2 fused with the N-terminal SP sequence of Avr1b, which has been reported as a secretory leader and was used as a positive control, grew on both the CMD-W medium and YPRAA medium. Similar to the positive control Avr1b, the predicted SPs of these eight SmCSEPs, which suppressed the BT-PCD and INF1-mediated PCD, enabled the invertase mutant yeast strain to grow on CMD-W medium and YPRAA medium (Fig. 3). Additionally, a triphenyl tetrazolium chloride (TTC) color reaction was performed to determine whether the predicted SPs had secretory functions. The N-terminal SPs of all eight SmCSEPs and Avr1b resulted in secretion of fructosidase SUC2 into the extracellular domain, reducing TTC and converting it to a dark red color. All the YSST results suggest that the putative N-terminal SPs of these eight SmCSEPs are functional and can guide the secretion of the truncated invertase, thus verifying these eight SmCSEPs are secreted by *S. musiva*.

Subcellular localization of SmCSEPs in planta

To characterize the subcellular localization of the eight SmCSEPs in planta, they were cloned, without SP, and fused to C-terminal yellow fluorescent protein (YFP), under the control of the CMV 35S promoter. Each of the resulting PEG101-SmCSEP-YFP constructs was transiently expressed in *N. benthamiana* leaf epidermal cells via agroinfiltration. Live-cell imaging revealed that the control PEG104 expressing only the YFP exhibited fluorescence throughout the whole cell (cytoplasm and nucleus), and all eight tested SmCSEPs generated detectable fluorescence signals in *N. benthamiana* epidermal cells, with no obvious sign of aggregation or degradation (Fig. 4). Four of these eight SmCSEPs, SmCSEP5, SmCSEP6, SmCSEP12, and SmCSEP27, had a non-informative distribution. Fluorescence was diffuse throughout the plant cytoplasm, cell membrane, and the nucleoplasm, similar to YFP expressed alone. However, SmCSEP2, SmCSEP10, SmCSEP13, and SmCSEP25 were specifically localized to numerous punctate structures that are likely plant organelles (Fig. 4). None of these were chloroplasts, which could be easily distinguished by their larger size and chlorophyll autofluorescence (Supplementary Fig. S2). SmCSEP2 was localized to the nucleus and small rapidly moving structures (white arrowheads), which resembled elements of the plant cytoskeleton (Fig. 4). SmCSEP10 mainly targeted the membrane and large cytosolic aggregates in the cytoplasm (red arrowheads), which may target components of *cis*-Golgi or endoplasmic reticulum (ER) structures (Fig. 4). SmCSEP13 was excluded from the plant nucleus and localized to large punctate structures in the cytoplasm (red arrowheads) and small punctate structures near the cell wall (yellow arrowheads), potentially mitochondria (Fig. 4). SmCSEP25 localized to clear punctate structures that overlapped with the cell membrane (yellow arrowheads) (Fig. 4).

Functional screening of virulence-associated SmCSEPs in *S. musiva*

To screen for virulence-associated SmCSEPs in *S. musiva*, we transiently expressed either pBIN-SmCSEP-FLAG vector or pBIN empty vector (EV) control in different positions on *N. benthamiana* leaves via agroinfiltration. The sites of infiltration were subsequently inoculated with mycelial plugs of *F. proliferatum.* Based on the development of a tobacco–*F. proliferatum* pathosystem (Li et al. 2017; Qian et al. 2022), *F. proliferatum* infects and causes visible disease lesions on *N. benthamiana*. At 3 days post-agroinfiltration (dpa), the lesion areas estimated by ImageJ were used as an indicator of plant susceptibility. Among the eight SmCSEPs tested, we found that the expression of six SmCSEPs (SmCSEP2, SmCSEP5, SmCSEP10, SmCSEP13, SmCSEP25, and SmCSEP27) in one-half of *N. benthamiana* leaves exhibited larger lesions, indicating increased susceptibility to *F. proliferatum* compared with the expression of the EV control (Fig. 5). Expression of SmCSEP6 and SmCSEP12 had no obvious effect on the susceptibility to *F. proliferatum* (Fig. 5). These results clearly suggest that the transient expression of six SmCSEPs (SmCSEP2, SmCSEP5, SmCSEP10, SmCSEP13, SmCSEP25, and SmCSEP27) enhance the susceptibility of *N. benthamiana* to *F. proliferatum.*

Expression patterns of six virulence-associated *SmCSEP*s during *S. musiva* infection on poplar

Expression profiles of the six virulence-associated *SmCSEP*s were monitored by qRT-PCR analysis during *S. musiva* interactions with the susceptible poplar genotype BESC367. *SmCSEP2*, *SmCSEP5*, *SmCSEP13*, and *SmCSEP25* were upregulated across all time points, peaking at 72 hpi. In contrast, the expressions of *SmCSEP10* and *SmCSEP27* peaked at 24 hpi, decreasing at 72 hpi. *SmCSEP10* and *SmCSEP27* followed a similar pattern, with a higher peak at 24 hpi and a sharper decline

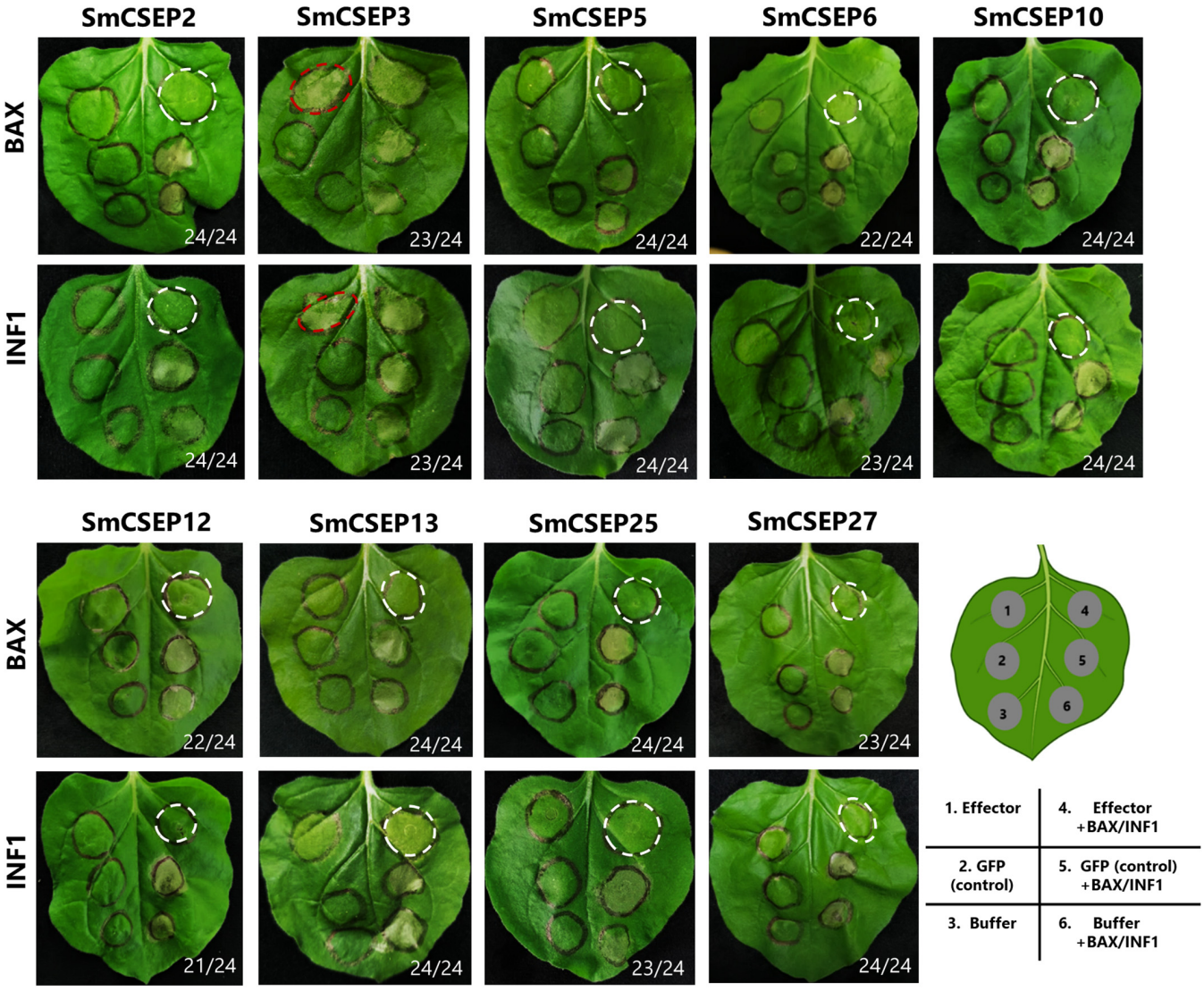

Fig. 2. Transient expression of SmCSEPs in *Nicotiana benthamiana* suppressed programmed cell death triggered by BAX and PAMP-INF1. *N. benthamiana* leaves were infiltrated with buffer and *Agrobacterium* cells containing each tested SmCSEP or pGR107::green fluorescent protein (GFP) (as a control). Agroinfiltration sites of each *N. benthamiana* leaf expressing each SmCSEP, GFP, and buffer were either performed alone or followed 24 h later by infiltration with *Agrobacterium* cells carrying either pGR107::BAX (top) or pGR107:: INF1 (bottom), respectively. The schematic diagram in the lower right corner depicts the positions of SmCSEPs, GFP, buffer, and each challenge with BAX or INF1 in the infiltration sites on each *N. benthamiana* leaf. Representative photos of plants exhibiting suppressed cell death responses were taken 3 days after infiltration. The experiments were repeated at least three times, and each replicate included eight plants. Numbers, for example, 23/24, indicate that 23 of 24 infiltrated leaves in infiltration site no. 4 (white dashed lines) exhibited phenotypes of suppressing BAX- or INF1-triggered cell death or 23 of 24 infiltrated leaves in infiltration site no. 1 (red dashed lines) exhibited phenotypes of inducing programmed cell death.

by 72 hpi. The expression profiles across the time points (Fig. 6) were consistent with those of the RNA-Seq (Fig. 1).

Certain SmCSEPs suppress chitin-triggered ROS generation in *N. benthamiana*

SmCSEP suppression of the chitin-triggered ROS burst in *N. benthamiana* revealed that SmCSEP2, SmCSEP13, and SmCSEP25 suppressed ROS production triggered by chitin, in contrast with the negative control enhanced GFP (eGFP) (Fig. 7), demonstrating that SmCSEP2, SmCSEP13, and SmCSEP25 can suppresses chitin-induced PTI.

Certain SmCSEPs suppress chitin-elicited callose deposition in *N. benthamiana*

Callose formation in tobacco leaves transiently expressing each of the six SmCSEPs and the negative control eGFP were treated with chitin. We observed a significant reduction (>50%) in callose deposition, elicited by chitin, in leaves pre-infiltrated with SmCSEP2, SmCSEP13, and SmCSEP25. In contrast, the remaining three SmCSEPs did not suppress callose deposition (Fig. 8). In addition, SmCSEP2, SmCSEP13, and SmCSEP25 also suppressed HR triggered by the PAMP elicitor INF1 (Fig. 2A), suggesting that SmCSEP2, SmCSEP13, and SmCSEP25 can suppress multiple PTI responses in *N. benthamiana*. In contrast, water-treated control leaves expressing eGFP or the six SmCSEPs did not produce callose in *N. benthamiana* (Supplementary Fig. S4).

Discussion

Pathogen CSEPs play a diversity of roles in plant–pathogen interactions. This diversity of function corresponds to sequence diversity and a lack of conserved features common to CSEPs. The lack of sequence conservation has confounded efforts for efficient prediction of effector function and resulted in a broad set of criteria used to select putative CSEPs for functional characterization (De Wit et al. 2009; Figueroa et al. 2021; Jaswal et al. 2020; Selin et al. 2016; Stergiopoulos and de Wit 2009). To circumvent the lack of sequence conservation, pathogen genomes and sophisticated computational approaches are increasingly being leveraged for effector prediction (Chen et al. 2018b; Dalio et al. 2018; Dong et al. 2015; Haas et al. 2009; Huang et al. 2022; Lorrain et al. 2015; Zhang et al. 2021a). For example, a preliminary search for CSEPs among the 10,156 predicted protein-coding genes in the reference genome of *S. musiva* predicted 142 candidate effectors (Tabima et al. 2020). This relatively large number of candidates can be further reduced for potential characterization using expression patterns during infection (Lo Presti et al. 2015). This approach has been used to identify putative effectors in a variety of plant pathogens, such as *P. sojae* (Wang et al. 2011), *P. oryzae* (Chen et al. 2013; Dong et al. 2015), *Puccinia triticina* (Zhang et al. 2020), *Melampsora larici-populina* (Lorrain et al. 2015), *Ustilago hordei* (Ökmen et al. 2018), *Elsinoë ampelina* (Li et al. 2021), and *Marssonina brunnea* (Cheng et al. 2014). Applying this methodology to the *S. musiva*–poplar interaction reduced the number of predicted SmCSEPs to 28.

One hallmark of many fungal CSEPs is the presence of an N-terminal SP. Among the 28 SmCSEPs, four (SmCSEP11, SmCSEP15, SmCSEP17, and SmCSEP19) lacked a predicted N-terminal SP (Supplementary Table S4). Secretion of the remaining 24 SmCSEPs was tested using an YSST assay that confirmed secretion of 19 SmCSEPs. However, it is important to note that all 28 SmCSEPs were predicted to be effectors (Supplementary Table S4) and could in fact be secreted through pathways other than the conventional ER–Golgi apparatus route. Accumulating evidence suggests that novel secretion pathways used by fungal plant pathogens exist (Giraldo et al. 2013; Reindl et al. 2019): for example, the VdIsc1 effector from *Verticillium dahliae* (Liu et al. 2014), the avirulence proteins (AVR_{a10} and AVR_{k1}) from the barley powdery mildew fungus *Blumeria graminis* f. sp. *hordei* (Ridout et al. 2006), and the peroxisomal sterol carrier protein (Scp2) from the corn smut fungus *Ustilago maydis* (Krombach et al. 2018). However, in the current study, we focused on SmCSEPs with verified secretion and lacking any predicted TMDs. In future work, it could prove interesting to evaluate *S. musiva* culture filtrates using proteomic analysis to determine whether the four predicted effectors, lacking an N-terminal SP, are in fact secreted.

The selection of SmCSEPs for further characterization can also use a population genetics approach. For example, to evade recognition by plant *R* genes or adapt to the host, effector genes evolve rapidly in pathogen populations, resulting in a signal of diversifying selection (Fouché et al. 2018; Sánchez-Vallet

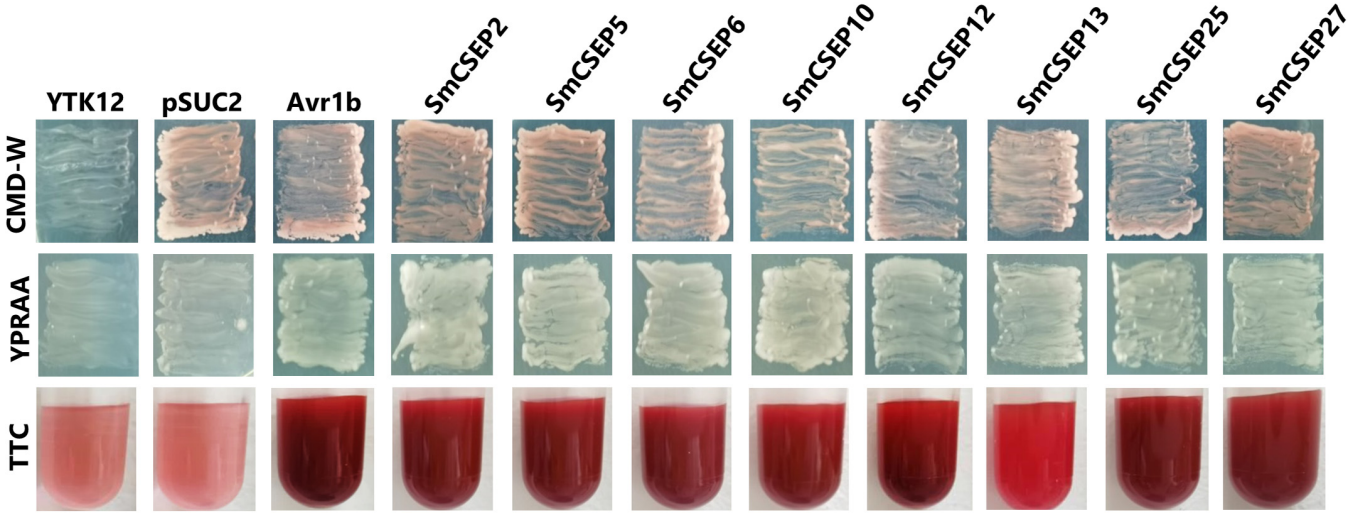

Fig. 3. Functional validation of signal peptides (SPs) of eight programmed cell death–suppressed SmCSEPs using a yeast invertase secretion assay. The SP of each SmCSEP was fused into the pSUC2 vector and transformed into the yeast YTK12 strain. The predicted SP of pSUC2-Avr1b was used as a positive control. Non-transformed YTK12 and YTK12 carrying the pSUC2 vector were used as negative controls. Yeast growth on CMD-W (lacking tryptophan) medium confirmed that the vector was transformed into the yeast strain, while growth on YPRAA medium and triphenyl tetrazolium chloride (TTC) color change confirmed invertase secretion.

et al. 2018). While 8 SmCSEPs were not polymorphic with the *S. musiva* reference genome, the remaining 11 exhibited insertion/substitution polymorphisms (Supplementary Table S3), indicating that they may be under diversifying selection. In the population genomic analysis of 122 *S. musiva* isolates in North America, reduced sequence diversity in predicted effectors was correlated with reduced aggressiveness on *P. trichocarpa* (Tabima et al. 2020). Similar analyses in other plant pathogen populations indicate that pathogens deploy both conserved effectors and a repertoire of variable effectors, potentially mediating virulence across host plants (Baltrus et al. 2011; Chavarro-Carrero et al. 2021; Ebert et al. 2021; Terauchi and Yoshida 2010). Although all 19 SmCSEPs may play a role in virulence, the subset of 11 SmCSEPs with polymorphisms may be of particular interest.

Many effectors from different pathogens have been shown to possess the same capacity to induce or suppress cell death in both non-host and host plants (Chen et al. 2018a). Two examples include the *P. sojae* apoplastic effector PsXEG1 (Ma et al. 2015) and HopPtoN, a member of type III secretion system of effectors (López-Solanilla et al. 2004). To leverage effector redundancy across host and none-host plants, complementing the in silico predictions, we carried out in planta assays in a heterologous system. The 19 SmCSEPs were screened using an *Agrobacterium*-mediated transient expression assay in the non-host *N. benthamiana*. Eight out of 19 tested SmCSEPs (SmCSEP2, SmCSEP5, SmCSEP6, SmCSEP10, SmCSEP12, SmCSEP13, SmCSEP25, and SmCSEP27) suppress PCD triggered by the mouse elicitor BAX and the oomycete PAMP INF1 (Fig. 2). Only SmCSEP3 triggered cell death in *N. benthamiana* (Fig. 2), suggesting that SmCSEP3 is the first necrosis-inducing protein reported for *S. musiva*. Domain prediction contrasting PCD suppressing/inducing SmCSEPs revealed that SmCSEP2 and SmCSEP3 both contain a glycoside hydrolase (GH) family domain (Supplementary Table S3). However, they differ from each other in their ability to induce or suppress cell death (Fig. 2). The carbohydrate-active enzymes database indicates that SmCSEP3 possesses a GH43 domain (amino acids 25 to 311) with multifunctional α-L-arabinofuranosidase, β-D-xylosidase, α-L-arabinanase, and β-D-galactosidase activities. However, SmCSEP2 possessing a GH128 domain (amino acids 29 to 266) has β-1,3-glucanase and β-1,3-glucosidase activities. SmCSEPs possessing different GH family domains with different enzyme activities may explain why the cell-death suppression/induction activity varied between SmCSEP2 and SmCSEP3.

The roles of cell wall-degrading enzymes belonging to several GH families have recently been demonstrated to have roles in invasion, pathogenicity, and virulence of fungi and oomycetes

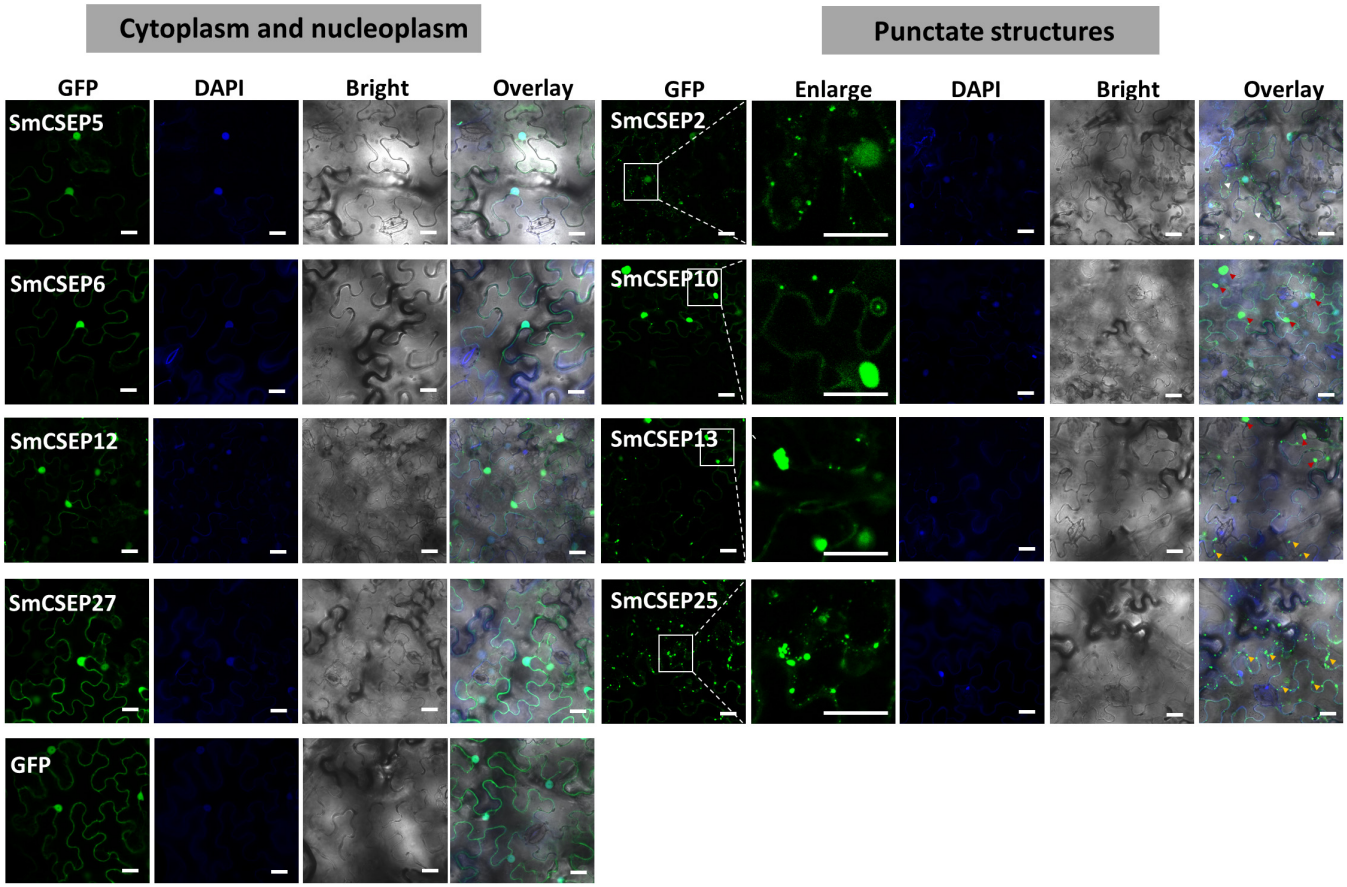

Fig. 4. Subcellular localization of eight SmCSEPs in *Nicotiana benthamiana* leaf cells. A total of eight yellow fluorescent protein (YFP)-tagged SmCSEPs were transiently expressed in *N. benthamiana* leaf cells by agroinfiltration. Live-cell imaging was performed with a laser-scanning confocal microscope 2 days after infiltration. The localization of the plant nucleus was detected by DAPI (4′,6-diamidino-2-phenylindole) staining. Green fluorescent protein (GFP) and DAPI were excited at 488 nm and 405 nm, respectively. GFP (green) and DAPI (blue) fluorescence was collected at 505 to 525 nm and 440 to 475 nm, respectively. Bright: field of bright light; Enlarge: enlarged images of the white square area in GFP channels; Overlay: merge with the three former images. PEG104 expressing only the YFP was used as a GFP control. Noninformative distribution, in which the GFP signal diffused throughout the plant cytoplasm and the nucleoplasm, is indicated in the left panel, and specific cellular compartments in which the GFP signal accumulated are indicated in the right panel. White arrowheads indicate small, rapidly moving structures (SmCSEP2); red arrowheads indicate large cytosolic aggregates in the cytoplasm (SmCSEP10) and large punctate structures in the cytoplasm (SmCSEP13); yellow arrowheads indicate small punctate structures near the cell wall (SmCSEP13) or near the cell membrane (SmCSEP25). Scale bars: 20 μm.

(Bradley et al. 2022; Rafiei et al. 2021). For example, two GH10 xylanases from *Phytophthora parasitica*, ppxyn1 and ppxyn2, were found to be essential for virulence toward *N. benthamiana* and tomato plants (Lai and Liou 2018). Xyloglucanase (XEG1), a GH12 protein from *P. sojae*, *V. dahliae*, *Botrytis cinerea*, *Fusarium oxysporum*, and several other fungi, can contribute to virulence and act as a PAMP to trigger cell death and modulate plant immunity (Gui et al. 2017; Ma et al. 2015; Zhang et al. 2021b; Zhu et al. 2017). In contrast, a paralogous PsXEG1-like protein from *P. sojae*, PsXLP1, lost enzyme activity but binds to GmGIP1 (an apoplastic glucanase inhibitor protein from soybean) more tightly than does PsXEG1, thus freeing PsXEG1 to support *P. sojae* infection (Ma et al. 2017; Sun et al. 2022). The cell death-suppressing SmCSEP2 and cell death-inducing SmCSEP3 may also deploy the same apoplastic decoy strategy as the effector pair PsXEG1 and PsXLP1, disrupting plant defense.

Another effector pair of interest is SmCSEP5 and SmCSEP14, which both contain a domain with peptidyl-prolyl *cis/trans* isomerase (PPIase) activity (Supplementary Table S3). Although, SmCSEP5 encoding a cyclophilin-type PPIase (amino acids 39 to 196) could suppress BAX-triggered cell death and promote *F. proliferatum* infection on *N. benthamiana* leaves; SmCSEP14, encoding an FK506-binding protein (FKBP)-type PPIase (amino acids 34 to 126), could not (Figs. 2 and 5). PPIases have also been identified as virulence-associated proteins, including cyclophilins and FKBPs. So far, most identified and characterized virulence-associated FKBPs are from pathogenic bacteria (Meng et al. 2011; Ünal and Steinert 2015). In contrast to the bacterial FKBPs, fungal FKBPs suffer from a paucity of physiological data. The specific functions of FKBPs appear to vary dramatically among organisms. As a result, it is difficult to speculate about the potential role played by the FKBP-type PPIase of SmCSEP14 in *S. musiva*.

In contrast, the SmCSEP5 effector encoding a cyclophilin-type PPIase was found to suppress BAX-triggered cell death and promote *F. proliferatum* infection on *N. benthamiana*

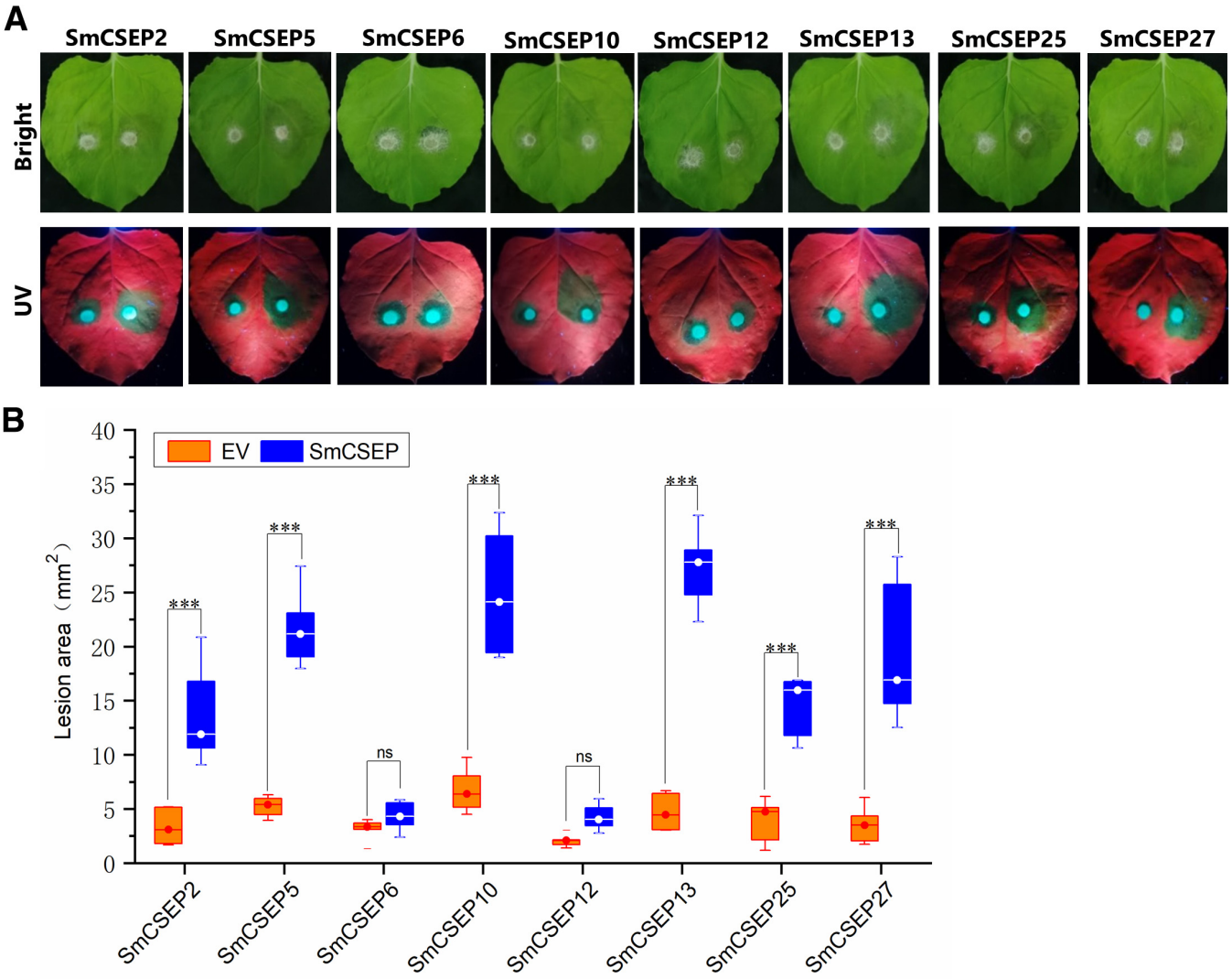

Fig. 5. Transient expression of six SmCSEPs in *Nicotiana benthamiana* enhanced the infection of *Fusarium proliferatum*. **A,** Increased lesion development of *F. proliferatum* on *N. benthamiana* when six of the tested eight SmCSEPs were transiently expressed. *N. benthamiana* leaves were infiltrated by *Agrobacterium tumefaciens* harboring the vector expressing each examined eight SmCSEPs in one half and the pBinFLAG empty vector (EV) in the other half. The infiltrated leaves were incubated for 24 h and subsequently inoculated with mycelial plugs of *F. proliferatum*. The photograph of disease symptoms was taken at 3 days post-agroinfiltration (dpa). Similar results were obtained from two additional experiments. **B,** Quantification of lesion areas on *N. benthamiana* leaves expressing each of the examined eight SmCSEPs or EV after *F. proliferatum* inoculation. Box plot diagrams show the mean lesion areas of *F. proliferatum*-inoculated tobacco leaves. Lesion areas at 3 days (A) were measured using ImageJ software for three independent biological replicates. Each replicate included at least five leaves (mean ± SD; $n = 18$). *P* values were from a Student's *t*-test: ***$P < 0.001$; ns, no significance. Dashes on box plots indicate 25th and 75th percentile outliers.

leaves, which is consistent with previous results showing that cyclophilin-encoding or cyclophilin-like genes have been reported to contribute to pathogenicity in several pathogenic fungi from animals to plants, including the human pathogenic fungus *Cryptococcus neoformans* (Wang et al. 2001), the rice blast fungus *Magnaporthe grisea* (Viaud et al. 2002), the gray mold fungus *B. cinerea* (Sun et al. 2021; Viaud et al. 2003), the chestnut blight fungus *Cryphonectria parasitica* (Chen et al. 2011), and the entomopathogenic fungus *Beauveria bassiana* (Zhou et al. 2016). Hence, it will be interesting to examine whether SmCSEP5 is enzymatically active and the extent to which it contributes to virulence. This is likely dependent on PPIase activities in *S. musiva*.

Cyclophilins have been discovered in plants and could serve as host targets of pathogen effectors. For example, AvrRpt2, an effector from *Pseudomonas syringae*, was delivered into the plant cell as an inactive form and subsequently activated by *Arabidopsis* cyclophilin ROC1 (Coaker et al. 2005). In soybean, a cyclophilin protein GmCYP1 physically interacts with the *Phytophthora* effector Avr3b and acts as a "helper" to activate the nudix hydrolase activity of Avr3b, which is required for the full virulence of *P. sojae* (Kong et al. 2015). These findings suggest that the SmCSEP5 effectors encoding a cyclophilin-type PPIase may also function in a similar manner, interfering with the host immunity. Simultaneously, the different PPIase activities or PPIase types possessed by SmCSEP5 and SmCSEP14 might affect the outcome of the interaction between *S. musiva* and poplars. One approach to address the function of the cyclophilins and FKBPs will be to identify the targets of SmCSEP5 and SmCSEP14, respectively, by yeast two-hybrid assays and tandem affinity purification–mass spectroscopy. These studies are currently underway.

Suppression of PCD by SmCSEPs was a common feature of these assays. For example, the expression of three out of the six PCD-suppressing effectors, SmCSEP2, SmCSEP13, and SmCSEP25, suppressed both the chitin-triggered ROS burst (Fig. 7) and callose deposition (Fig. 8) in *N. benthamiana.* Transient expression of these effectors also conferred enhanced susceptibility of *N. benthamiana* to *F. proliferatum* (Fig. 2), suggesting that SmCSEP2, SmCSEP13, and SmCSEP25 contribute to virulence by suppressing PTI. In addition, we tested PTI activation by using a second bacterial PAMP, flg22. The flg22-triggered ROS burst (Supplementary Fig. S3) and callose deposition (Supplementary Fig. S5) were effectively suppressed following transient expression of SmCSEP2, SmCSEP10, and SmCSEP27 in tobacco leaves, followed by flg22 treatment. SmCSEP13 and SmCSEP25 only suppressed chitin-induced PTI and not flg22-induced PTI, whereas SmCSEP10 and SmCSEP27 only suppressed flag22-induced PTI but not chitin-induced PTI. Four of these effectors, SmCSEP2, SmCSEP10, SmCSEP13, and SmCSEP25, were localized to punctate structures within the plant cells. We considered it likely that small, actively moving

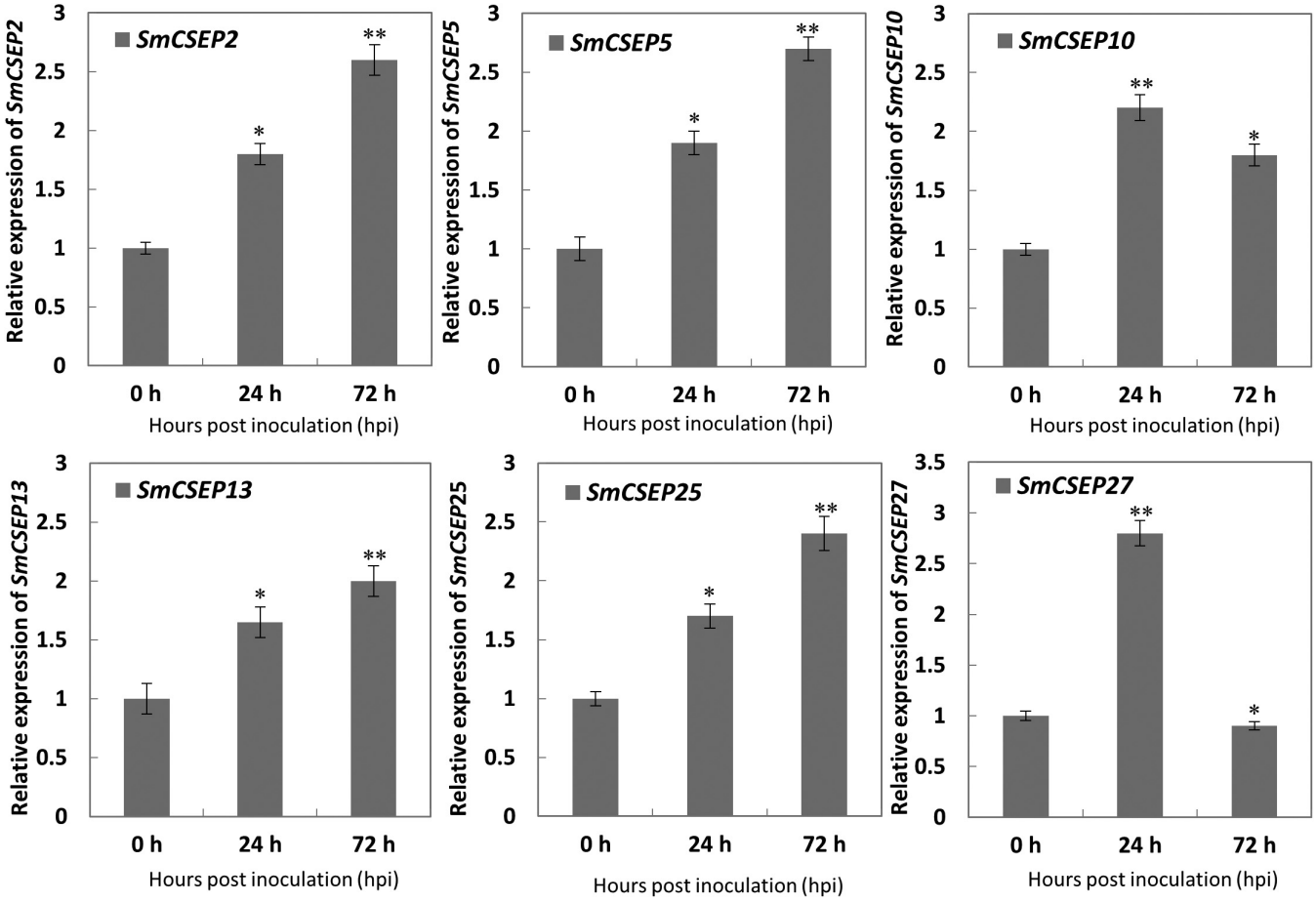

Fig. 6. Transcript abundances of six virulence-associated *SmCSEP*s in *Sphaerulina musiva*-infected poplar leaves. The susceptible poplar genotype BESC367 was inoculated with mycelial plugs of *S. musiva* isolate MN-14. Inoculated stem tissues were collected at 0, 24, and 72 h postinoculation. Three biological replicates were performed for each time point. A total of nine trees were used in this experiment (3 time points × 3 biological replicates). For each time point, six stems per tree were collected as one sample. Relative expression levels of six virulence-associated *SmCSEP*s (*SmCSEP2*, *SmCSEP5*, *SmCSEP10*, *SmCSEP13*, *SmCSEP25*, and *SmCSEP27*) were determined by qRT-PCR and normalized against the expression of the *S. musiva* endogenous *actin-1* gene. Values are means ± standard deviations (as error bars) ($n = 3$). This experiment was repeated three times with similar results. Asterisks indicate significant differences in gene expression level relative to the 0-hpi baseline; *P* values were from a Student's *t*-test: $*P < 0.05$; $**P < 0.001$.

punctate structures (white arrowheads in Fig. 4) observed in SmCSEP2 were elements of the plant cytoskeleton, and large cytosolic aggregates in the cytoplasm (red arrowheads in Fig. 4), whereas SmCSEP10 and SmCSEP13 were localized to components of *cis*-Golgi or ER. These results suggest that these effectors inhibit PTI responses and contribute to virulence in markedly different ways in *N. benthamiana* and provide further evidence for the different roles of these effectors in modulating plant immunity.

The integrated genomic and transcriptomics approach described in this study effectively identified in planta–expressed effectors from *S. musiva* for functional characterization. For the first time, in planta functional analysis and subcellular localization of *S. musiva* candidate effector proteins has been described. These results provide clues to the molecular mechanisms of pathogenicity in the *S. musiva*–poplar interaction. Although, we relied on a heterologous system to test the function of these effectors, subsequent work could be conducted in poplar. However, given the well-described recalcitrance of poplar to transformation and regeneration, this may prove difficult and time-consuming (Ma et al. 2022a, b; Strauss et al. 2022). The next step will be to identify the potential SmCSEP-interacting protein(s) to reveal the functions of SmCSEP in *S. musiva*–poplar interaction to develop a better understanding of the biological functions of SmCSEPs.

Materials and Methods

Culture of fungal and bacterial strains

The *S. musiva* isolate MN-14 (collected from a commercial fiber farm nursery near Belle River in Minnesota, 45.97°N, 95.19°W) was stored as plugs on K-V8 agar (180 ml V8 Vegetable Juice, Campbell Soup Company, Camden, NJ, U.S.A.; 2 g $CaCO_3$; 20 g agar; and 820 ml H_2O) in 50% glycerol at –80°C. Two weeks before inoculations, two cryotubes of the stored isolate were poured onto K-V8 agar Petri plates and maintained for 12 days under continuous light at room temperature. *F. proliferatum* isolate JN6-8 was maintained on potato dextrose agar and cultured for 4 days in continuous darkness at room temperature. *Escherichia coli* and *Agrobacterium tumefaciens* GV3101 were cultured in Luria–Bertani with the addition of different antibiotics (kanamycin: 50 mg/liter; gentamycin: 20 mg/liter; rifampicin: 50 mg/liter).

Plant growth conditions

Three susceptible *P. trichocarpa* genotypes (BESC367, BESC347, and GW9807) were used in the experiments. A total of 12 dormant branch cuttings, 10 cm in length, for each genotype, were planted in Super Cone-tainers (Ray Leach SC10 Super Cone-tainers, Stuewe and Sons, Tangent, OR, U.S.A.) measuring 3.8-cm in diameter and 21-cm deep and filled with growing medium (SunGro Professional Mix no. 8, SunGro Horticulture, Agawam, MA, U.S.A.) combined with slow-release Nutricote fertilizer (15-9-12) (N-P-K) (Osmocote Plus, Scotts Company, Marysville, OH, U.S.A.). Trees were grown in a greenhouse with an 18-h photoperiod augmented with sodium lamps and a temperature regime of 20/16°C (day/night). Trees were fertilized weekly with 20-20-20 liquid fertilizer (Scotts Peters Professional) until inoculation.

Seeds of *N. benthamiana* were germinated in a controlled growth chamber under a 16-h/8-h light/dark cycle at 25°C, with 60% relative humidity. Ten-day-old seedlings were then transferred into 4-inch plastic pots. One plant was maintained in

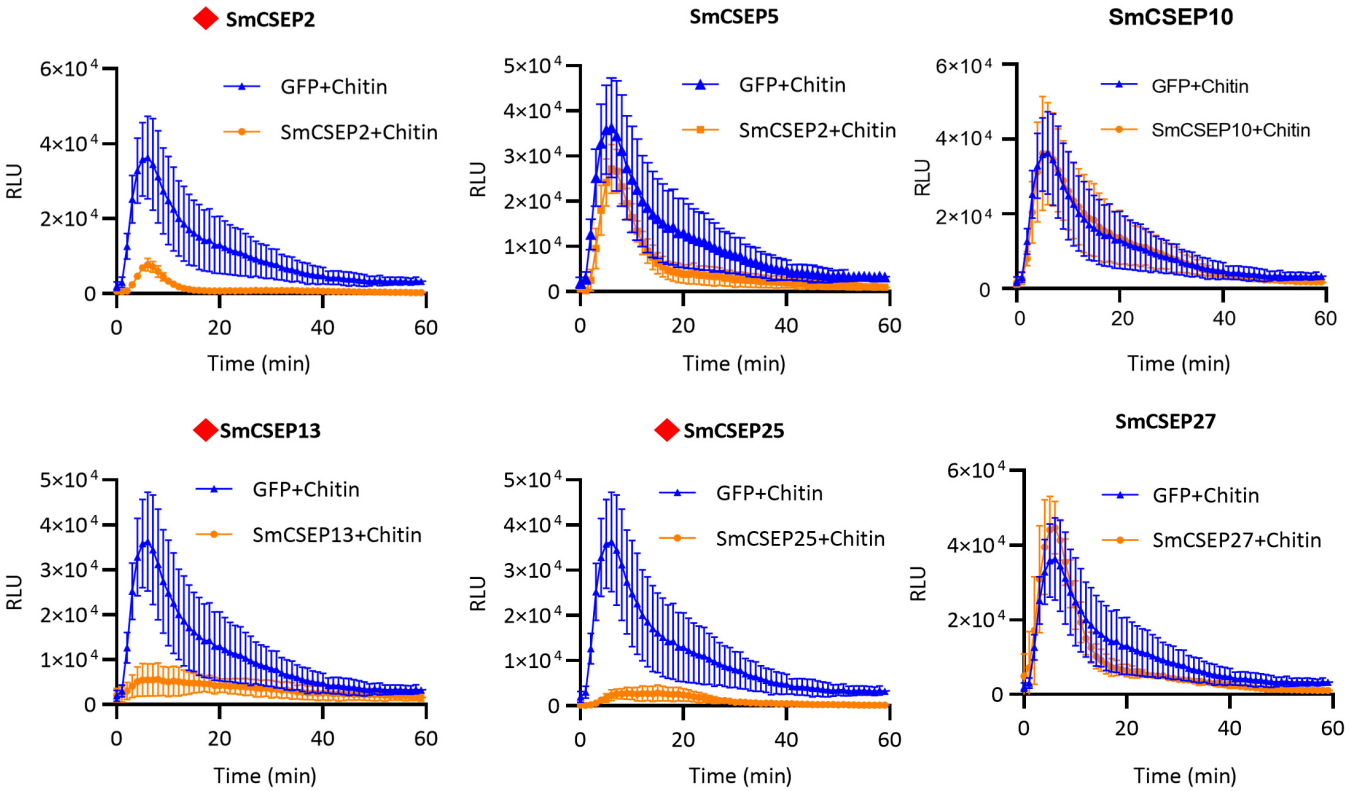

Fig. 7. Transient expression of three SmCSEPs inhibited the chitin-triggered reactive oxygen species (ROS) burst in *Nicotiana benthamiana*. The line graph shows the effects of transiently expressing six SmCSEPs in *N. benthamiana* on the chitin-triggered ROS burst. SmCSEPs with an inhibitory effect on chitin-triggered ROS are indicated with a red diamond. Leaf disks from *N. benthamiana* transiently expressing SmCSEP-FLAG or green fluorescent protein (GFP)-FLAG (negative control) were respectively treated with 500 µg/ml chitin. The total ROS production was measured by measuring the relative light units (RLU) over a period of 30 min with a luminol-chemiluminescence assay using a TECAN reader. Error bars represent the mean ± standard errors ($n = 12$) of three independent experiments with independent biological samples.

each pot. Four- to 5-week-old *N. benthamiana* plants were used for agroinfiltration.

Inoculation of three susceptible poplar genotypes for transcriptome sequencing

Inoculations were conducted by placing two 0.8-cm-diameter plugs of sporulating mycelium from isolate MN-14 on the stem of each tree at the midpoint. The plug was positioned directly over a lenticel and wrapped in Parafilm. Approximately 100 mg of stem tissue was collected at 0, 24, and 72 h; placed in lysing matrix tubes; and flash-frozen in liquid nitrogen. A separate tree was used for each time point. A mock-inoculated control was conducted by placing a water agar plug on the stem of each tree in an identical manner to that described above. As a fungal control, three 7-day-old fungal cultures of the MN-14 isolate were collected from liquid K-V8 media, placed in lysing matrix tubes, and flash-frozen in liquid nitrogen. The cultures were used as an in vitro control. Three biological replicates were performed for each time point and each genotype. A total of 36 trees were used in this experiment: [3 genotypes × (3 time points + 1 mock inoculation) × 3 biological replicates].

mRNA was extracted using the mRNA Dynabeads DIRECT Kit (Thermo Fisher Scientific, Waltham, MA, U.S.A.). Stranded cDNA libraries were generated using the Illumina TruSeq Stranded mRNA Library prep kit. Ten nanograms of mRNA was fragmented using divalent cations and high temperature. The fragmented RNA was reverse transcribed using random hexamers and SSII (Invitrogen, Thermo Fisher Scientific, Waltham, MA, U.S.A.) followed by second-strand synthesis. The fragmented cDNA was treated with end-pair, A-tailing, adapter ligation, and 8 cycles of PCR. The prepared libraries were then quantified using KAPA Illumina library quantification kit (KAPA Biosystems, Wilmington, MA, U.S.A.) and run on a Roche LightCycler 480 real-time PCR instrument. The quantified libraries were then multiplexed, and the pool of libraries was prepared for sequencing on the Illumina NovaSeq 6000 sequencing platform using NovaSeq XP v. 1 reagent kits (Illumina), S4 flow cell, following a 2 × 150 indexed run recipe. Reads were then mapped to both the *S. musiva* SO2202 v1.0 genome (http://genome.jgi-psf.org/pages/dynamicOrganismDownload.jsf?organism=Sepmu1) and *P. trichocarpa* genome v3.0/v10.1 (http://popgenie.org) using TopHat2 v. 2.0.14 (Kim et al. 2013). The expression level was estimated using the read counts per million (CPM) calculation in the CLC Genomics workbench (Qiagen, Redwood City, CA, U.S.A.). Comparisons were made between the 24-hpi and 72-hpi treatments and the 0-hpi control. All raw data are available in GenBank under SRA accession IDs SRP 240491, 240493, 240494/240492, 240496, 240497/240495, 240498, 240500/240499, 240501, 240502 (corresponding to BESC367_Control/0 hpi/24 hpi/72 hpi), SRP 240482, 240489/240490, 240484, 240480/240485, 240488, 240487/240486, 240483, 240481 (corresponding to BESC347_Control/0 hpi/24 hpi/72 hpi), and SRP 240527, 240519, 240524/240523, 240522, 240520/240528, 240525, 240521/240526, 240518, 240517(corresponding to GW9807_ Control/0 hpi/24 hpi/72 hpi). Heat maps were produced using the R package pheatmap v. 1.0.12 (https://cran.r-project.org/web/packages/pheatmap/index.html) (Barter and Yu 2018).

Selection of candidate effector proteins of *S. musiva* for further experimental analysis

A total of 142 putative effectors of *S. musiva* were previously predicted by Tabima et al. (2020). Combined with the transcriptomic analysis (Supplementary Table S1), a total of 28 putative effector candidates were selected for the following analysis. The workflow for effector prediction (Fig. 9) describes the procedure. The N-terminal SPs of these proteins were initially predicted using SignalP v. 3.0 and confirmed with SignalP v. 5.0 (http://www.cbs.dtu.dk/services/SignalP) with a minimum

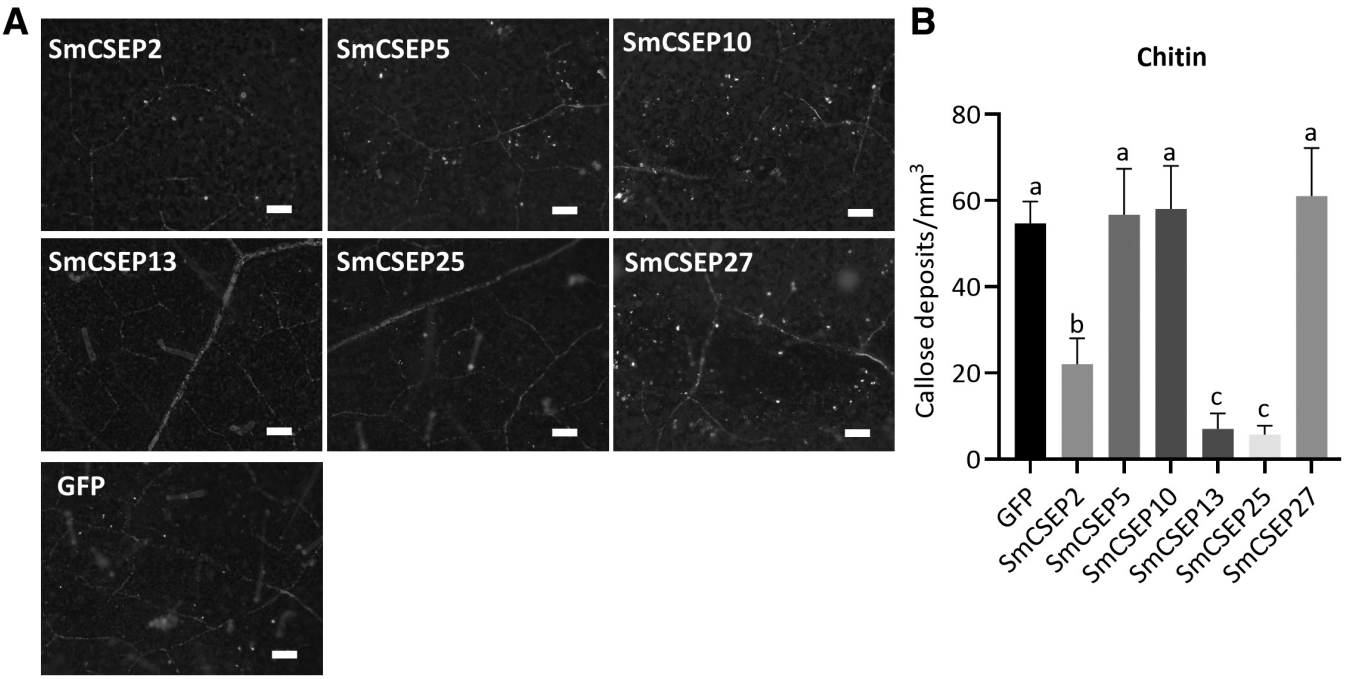

Fig. 8. Transiently expression of three SmCSEPs inhibited the chitin-triggered callose deposition in *Nicotiana N. benthamiana*. **A,** Morphologic differences between chitin-elicited callose depositions in *N. benthamiana* leaves transiently expressing green fluorescent protein (GFP; negative control) and each of the six SmCSEPs. The leaves were then stained with aniline blue for callose deposits at 48 h postinfiltration and observed by fluorescence microscopy. Scale bars: indicate 200 μm. **B,** Quantification of callose deposits per leaf area (mm^2) in GFP- and each SmCSEP-expressing *N. benthamiana* leaves using ImageJ software. Error bars represent the mean ± standard errors ($n = 12$) from three leaves of each plant and three independent experiments. Different letters indicate statistically significant differences between treatments (Fisher's least significant differences test; $\alpha = 0.05$).

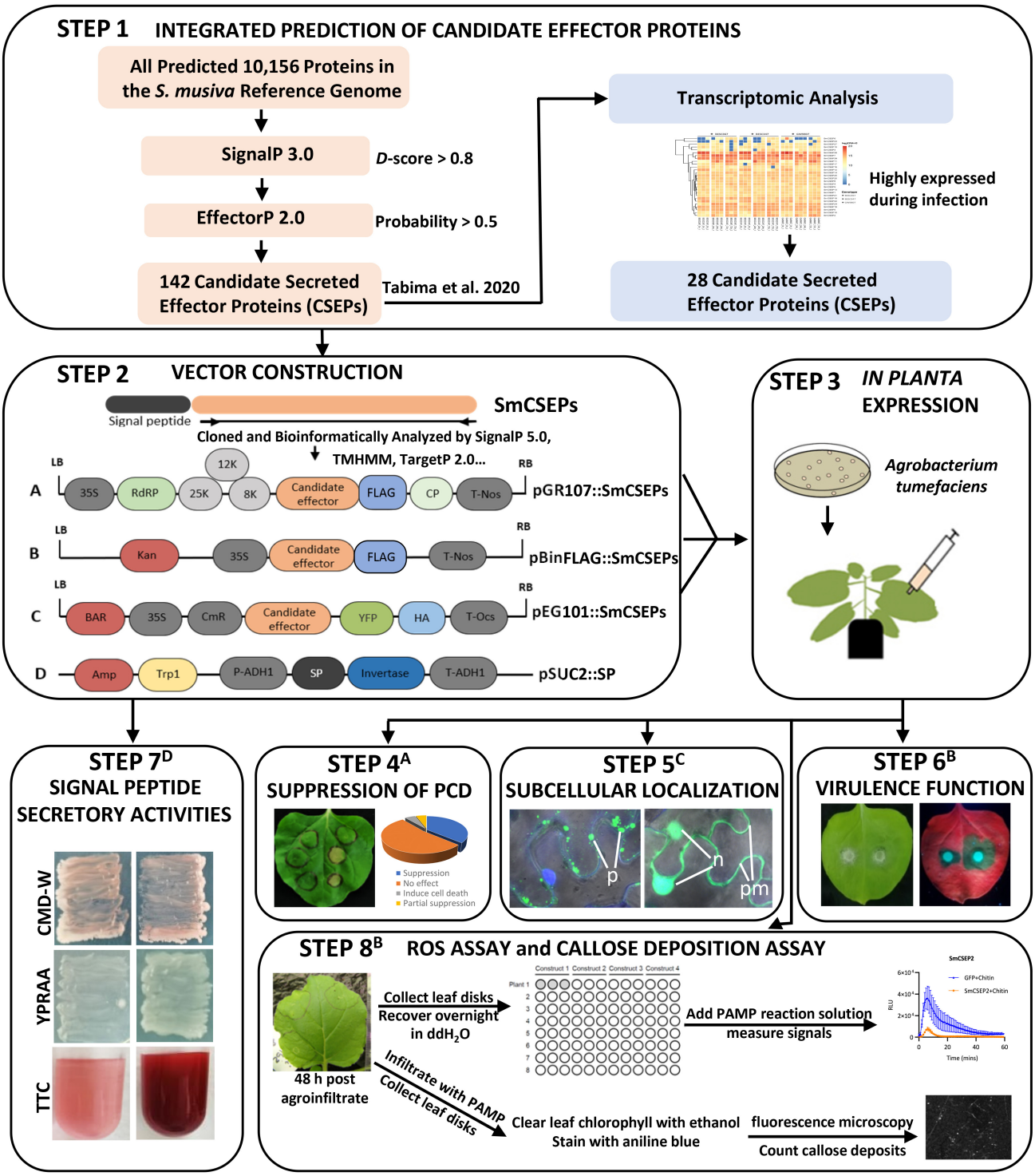

Fig. 9. Workflow used for prediction and experimental function analysis of *Sphaerulina musiva* candidate secreted effector proteins (SmCSEPs). **Step 1,** Identifying and selecting candidate secreted effector proteins (CSEPs) of *S. musiva* using a combination of genomic and transcriptomic analyses. A total of 142 SmCSEPs were previously mined from a set of 10,156 predicted proteins in the *S. musiva* SO2202 v.1.0 reference genome via SignalP 3.0 and EffectorP 2.0 software (light red) (Tabima et al. 2020). Based on RNA sequencing (RNA-Seq) data, 28 SmCSEPs upregulated during infection were finally selected (light blue) for further functional analysis. **Step 2,** Constructing vectors for experimental function analysis of SmCSEPs. The sequences encoding mature forms of each SmCSEPs were cloned; sequenced; bioinformatically analyzed by SignalP 5.0, TargetP 2.0, TMHMM, ProtParam, and so on; and subcloned into pGR107 (A), pBinFLAG (B), and pEG101 (C) vectors, respectively. The predicted signal peptide (SP, dark)-encoding sequences of each SmCSEPs were fused in the vector pSUC2 (D). **Step 3,** The constructed pGR107-SmCSEPs (A), pBinFLAG-SmCSEPs (B), and pEG101-SmCSEPs (C) vectors were transiently expressed in *Nicotiana benthamiana* leaves by agroinfiltration. **Step 4^{A},** Suppressing BAX- or INF1-triggered programmed cell death (PCD) in *N. benthamiana* by SmCSEPs (example: SmCSEP25). The pie chart depicts the proportion of the tested SmCSEPs that induce PCD, suppress BAX- or INF1-triggered cell death, and have no effect on *N. benthamiana* leaves. **Step 5^{C},** The subcellular localization of SmCSEPs was determined by live-cell imaging with a laser-scanning confocal microscope. The illustration is an overlay image of a green fluorescent protein (GFP) diffusing in the plasma membrane (pm), nucleus (n), and punctate structures (p). **Step 6^{B},** Functional screening of virulence-associated SmCSEPs in *S. musiva*. **Step 7^{D},** Secretion validation of the SmCSEPs SPs by the yeast signal sequence trap (YSST) system. **Step 8^{B},** Suppressing chitin- or flg22-triggered reactive oxygen species (ROS) generation and callose deposition in *N. benthamiana* by SmCSEPs (example: SmCSEP2). ROS were monitored using a chemiluminescence assay with luminol as a substrate. Callose deposition was measured with the use of aniline blue staining and fluorescence microscopy. PAMP, pathogen-associated molecular pattern.

threshold D score > 0.8. The TargetP v. 2.0 (https://services.healthtech.dtu.dk/service.php?TargetP-2.0) was used to predict the potential subcellular localization in planta for each effector. The ExPasy ProtParam tool (https://web.expasy.org/protparam) was used to calculate the number of cysteine (Cys) residues. Furthermore, protein TMDs were predicted using TMHMM v. 2.0 (http://www.cbs.dtu.dk/services/TMHMM). The final list of putative effectors of S. *musiva* was selected based on the results of the prediction algorithms above and used in the subsequent experiments.

Cloning procedures and plasmid construction

To determine the cell death-inducing or cell death-inhibiting activity, the coding sequences of candidate effectors (without an SP) were amplified from the cDNA of *S. musiva* isolate MN-14 using the gene-specific primer pairs (pGR107-SmCSEP-F/pGR107-SmCSEP-R) (Supplementary Table S2). The amplicons were then inserted separately into the *Potato virus X* (PVX) vector pGR107 (Ma et al. 2015) with a FLAG-tag fused at the C-terminus by the method of digestion and connection using a ClonExpress II One Step Cloning kit (Vazyme Biotech, Nanjing, China), resulting in pGR107-SmCSEP-FLAG.

To characterize the subcellular localization of candidate effectors in *N. benthamiana*, the fragments of each SmCSEP were amplified from the pGR107-SmCSEP-FLAG with the indicated primers (Supplementary Table S2) and introduced into the pDONR207 vector (Invitrogen, Thermo Fisher Scientific) by BP recombination reactions, and then recombined by LR reactions into the destination vector pEG101 using Gateway technology (Earley et al. 2006). The final vector was named pEG101-SmCSEP-YFP-HA.

To investigate the virulence function of candidate effectors in *N. benthamiana* using an ROS assay, the pBinFLAG plasmid was used to generate pBin-SmCSEP-FLAG using the same method as that used for pGR107-SmCSEP with the following primer set: pBin-SmCSEP-universal-F/pBin-SmCSEP-universal-R. The universal primer is designed based on a 5′ and 3′ flanking sequence of SmCSEPs in the pEG101 vectors. All SmCSEPs were amplified with universal primers and inserted into pBIN-FLAG using a ClonExpress II One Step Cloning kit (Vazyme Biotech).

For functional assays of the SPs in yeast, the predicted SP-encoding sequences of the selected candidate effectors were fused in frame to the secretion-defective invertase gene in the vector pSUC2 (Jacobs et al. 1997) to form the recombinant construct pSUC2-SmCSEP-SP. All recombination constructs were verified by sequencing. Primers used in this study are listed in Supplementary Table S2.

Suppression assay of BAX- or INF1-induced cell death

For cell death suppression assays with the above constructs (pGR107-SmCSEPs-FLAG), we used *Agrobacterium*-based methods, as described by Yang et al. (2017). Each construct was transformed into *A. tumefaciens* strain GV3101 by the freeze-thaw method (Höfgen and Willmitzer 1988). The *Agrobacterium* cells were harvested by centrifugation (2,500 × g, 5 min) and then resuspended in $MgCl_2$ buffer (containing 10 mM $MgCl_2$, 10 mM MES, and 200 μM acetosyringone) until an OD_{600} of 0.4 was achieved, and then incubated in the dark for 3 h at 28°C before being infiltrated into *N. benthamiana* leaves using a 1-ml syringe. The left and right sides of *N. benthamiana* leaves were infiltrated with buffer (as a control) and *Agrobacterium* cells containing each tested SmCSEP or the negative control pGR107 EV, respectively. One day later, the same sites on the right sides of the leaves were re-infiltrated with *Agrobacterium* cells carrying either the pGR107-BAX or pGR107-INF1 constructs. To record the cell death phenotype, the leaves were continuously observed for up to 5 days. The experiment was repeated three times, and each replicate included eight plants.

Yeast signal sequence trap system

The functional validation of the predicted SPs of the selected candidate effectors was performed by the YSST system, as previously described (Jacobs et al. 1997). The pSUC2T7M13ORI (pSUC2) vector was used, which contains a SUC2 truncated invertase lacking both its own SP and the ATG start codon. The resulting pSUC2-SmCSEP-SP constructs were transformed into the *Saccharomyces cerevisiae* strain YTK12 while using a Frozen-EZ yeast transformation II kit (Zymo Research, Irvine, CA, U.S.A.), as previously described (Yin et al. 2018). All transformants were selected on yeast minimal medium with sucrose (CMD-W) (containing 0.67% yeast N base without amino acids, 0.075% tryptophan dropout supplement, 2% sucrose, 0.1% glucose, and 2% agar). Positive clones were also confirmed by PCR using vector-specific primers (Supplementary Table S2). The YTK12-positive clones with pSUC2 or the recombinant pSUC2 vectors were replica-plated onto YPRAA medium (1% yeast extract, 2% peptone, 2% raffinose, and 2 mg/ml antimycin A) for invertase secretion. The YTK12 strain transformed with the pSUC2 vector grows on the CMD-W medium, but not on the YPRAA medium. Negative controls included the untransformed YTK12 strain and the YTK12 strain transformed with the EV pSUC2. As a positive control, the YTK12 strain was transformed with pSUC2-Avr1b SP, the SP of the oomycete effector Avr1b from *P. sojae* that has been reported as a secretory leader (Dou et al. 2008). This experiment had three biological replicates. A TTC color reaction was additionally adopted to check whether the probable SPs exhibited secretory functions. Fructosidase SUC2 was secreted into the extracellular domain, reducing 2,3,5-triphenyl tetrazolium chloride (TTC) to red 1,3,5-triphenyl tetrazolium. To detect secreted invertase activity, the reduction of TTC to insoluble red 1,3,5-triphenyl tetrazolium was monitored.

Subcellular localization assay

A. tumefaciens cultures were infiltrated into *N. benthamiana* leaves in the manner described earlier with the following modifications. For achieving subcellular localization of each tested SmCSEP, the final OD_{600} was adjusted to 0.7. The *Agrobacterium* culture carrying the pEG101-SmCSEP-YFP vector was infiltrated at the same time as a pEG104 EV. Infiltrated leaves were maintained under the following conditions of low light and collected at 2 to 3 dpa for analysis under an LSM 710 laser-scanning microscope with the 20×, 40×, or 60× objective lens (Carl Zeiss, Shanghai, China). The *N. benthamiana* leaves were stained with 5 μg/ml DAPI (4′,6-diamidino-2-phenylindole) at 2 dpa. At 3 h after staining, the leaves were cut into 8 mm × 8 mm pieces and mounted in water on glass slides for confocal microscopy. The excitation wavelengths were set as follows: GFP (488 nm), chloroplast (488 nm), and DAPI (405 nm). GFP (green), chloroplast (red), and DAPI (blue) fluorescence was observed at 505 to 525 nm, 680 to 700 nm, and 440 to 475 nm, respectively. Scanning was performed in a sequential mode when required, and all the images obtained were those of single optical sections, with cells exhibiting moderate fluorescence intensity.

Virulence-enhancement assay

N. benthamiana leaves (4 to 5 weeks old) were infiltrated with a cell suspension of each *A. tumefaciens* at an optical density at 600 nm (OD_{600}) of 0.3. The *A. tumefaciens* strains harbor either the EV pBIN-FLAG or the vector pBIN-SmCSEP-FLAG expressing each examined SmCSEP. The infiltrated leaves were incubated for 24 h, after which mycelial plugs of a 4-day-old

F. proliferatum culture were inoculated onto the infiltrated areas of detached *N. benthamiana* leaves. Inoculated leaves were incubated at 25°C for 5 days on a 0.8% agar plate before lesions from *F. proliferatum* infection were measured. Experiments were repeated three times, and each replicate included at least five leaves. A quantitative assessment of lesion development was obtained using ImageJ software (https://imagej.nih.gov/ij) for three biological replicates.

qRT-PCR analysis

Expression of *SmCSEP* genes was quantified with qRT-PCR. The *S. musiva*-inoculated stem tissue samples were prepared as described above in the Materials and Methods section under "Inoculation of three susceptible poplar genotypes for transcriptome sequencing" and collected at 0, 24, and 72 hpi. For the 0-hpi samples, once all trees were inoculated, the inoculated stem tissue was collected and immediately frozen in liquid nitrogen. mRNA was extracted using the mRNA Dynabeads DIRECT Kit, as described earlier. First-strand cDNA was synthesized using SuperScript III First-Strand Synthesis SuperMix (Invitrogen), followed by qPCR using the iTaq Universal SYBR Green Supermix (Bio-Rad, Hercules, CA, U.S.A.). Gene-specific primers for each *SmCSEP* gene were designed and are listed in Supplementary Table S2. Three independent technical and biological replicates of each treatment were analyzed.

The *S. musiva* gene *actin-1* (GenBank accession no.: XM_016904422.1) was used as an endogenous reference control. The relative expression level of each gene was calculated using the comparative threshold ($2^{-\Delta\Delta C_T}$) method (Livak and Schmittgen 2001). The expression value of cDNA from 0-hpi samples was used for comparison. Statistical significance was determined using Student's *t*-test: $*P < 0.05$; $**P < 0.001$. This experiment was repeated three times.

ROS assay

ROS production was monitored using a luminol-based assay (Keppler et al. 1989). Leaves of 5-week-old *N. benthamiana* plants were infiltrated with *Agrobacterium* containing pBIN-SmCSEP-FLAG plasmid or pBIN-GFP-FLAG control (GFP). At 2 days after infiltration, leaf disks (5-mm diameter) were removed from the infiltrated area using a circular borer. The leaf disks were pre-incubated overnight in 96-well luminometer plates with distilled water. The leaves were drained carefully, and the water was discarded. It was replaced with 200 µl of a solution containing 35.4 µg/ml luminol (A8511-5g, Sigma-Aldrich, St. Louis, MO, U.S.A.) and 10 µg/ml horseradish peroxidase (P6782, Sigma-Aldrich). ROS was elicited with 100 nM flg22 or 500 µg/ml chitin (Genscript Biotech, Nanjing, China) or water for the mock controls in all experiments. Immediately after treatment, luminescence was measured in a TECAN infinite F200 micro-plate reader (TECAN, Männedorf, Switzerland).

Callose deposition assay

Callose deposition in infiltrated leaf disks at 48 h after infiltration was visualized after aniline blue staining, as described previously (Nguyen et al. 2010). Stained samples were viewed under an Olympus IX71 fluorescence microscope (Olympus, Tokyo, Japan). Fluorescence was observed under ultraviolet light (wavelength = 405 nm). The staining shows callose deposition as dots. After callose images were collected, fluorescence in the images was quantified with ImageJ software. Each experiment was repeated three times independently.

Acknowledgments

We are sincerely grateful to Qiang Cheng and Zhuge Qiang from Nanjing Forestry University for kindly sharing lab equipment. We also thank Yuanchao Wang from Nanjing Agricultural University for providing the pGR107, pGR107-GFP, pGR107-BAX, pGR107-INF1, and pBinFLAG, pBin-GFP-FLAG vectors; Danyu Shen for providing the pSUC2 vector and his excellent technical assistance in bioinformatics analysis; and Jie Huang for providing the *Fusarium proliferatum* isolate JN6-8.

Author-Recommended Internet Resources

S. musiva SO2202 v1.0 genome: http://genome.jgi-psf.org/pages/dynamicOrganismDownload.jsf?organism=Sepmu1
P. trichocarpa genome v3.0/v10.1: http://popgenie.org
Tophat2 v. 2.0.14: http://tophat.cbcb.umd.edu
Genesis v. 1.7.6: https://genome.tugraz.at/genesisclient/genesisclient_download.shtml
SignalP: http://www.cbs.dtu.dk/services/SignalP
TargetP: https://services.healthtech.dtu.dk/service.php?TargetP-2.0
ExPasy ProtParam: https://web.expasy.org/protparam
TMHMM: http://www.cbs.dtu.dk/services/TMHMM
R package pheatmap v. 1.0.12: https://cran.r-project.org/web/packages/pheatmap/index.html

Literature Cited

Ahmed, M. B., Santos, K. C. G. D., Sanchez, I. B., Petre, B., Lorrain, C., Plourde, M. B., Duplessis, S., Desgagné-Penix, I., and Germain, H. 2018. A rust fungal effector binds plant DNA and modulates transcription. Sci Rep. 8:14718.

Ares, A., and Gutierrez, L. 1996. Selection of poplar clones for the Lower Valley of the Colorado River, Argentina. Forestry 69:75-82.

Baltrus, D. A., Nishimura, M. T., Romanchuk, A., Chang, J. H., Mukhtar, M. S., Cherkis, K., Roach, J., Grant, S. R., Jones, C. D., and Dangl, J. L. 2011. Dynamic evolution of pathogenicity revealed by sequencing and comparative genomics of 19 *Pseudomonas syringae* isolates. PLoS Pathog. 7:e1002132.

Barter, R. L., and Yu, B. 2018. Superheat: An R package for creating beautiful and extendable heatmaps for visualizing complex data. J. Comput. Graph. Stat. 27:910-922.

Boller, T., and Felix, G. 2009. A renaissance of elicitors: Perception of microbe–associated molecular patterns and danger signals by pattern-recognition. Annu. Rev. Plant Biol. 60:379-406.

Bradley, E. L., Ökmen, B., Doehlemann, G., Henrissat, B., Bradshaw, R. E., and Mesarich, C. H. 2022. Secreted glycoside hydrolase proteins as effectors and invasion patterns of plant-associated fungi and oomycetes. Front. Plant. Sci. 13:853106.

Chavarro-Carrero, E. A., Vermeulen, J. P., Torres, D. E., Usami, T., Schouten, H. J., Bai, Y., Seidl, M. F., and Thomma, B. P. H. J. 2021. Comparative genomics reveals the *in planta*-secreted *Verticillium dahliae* Av2 effector protein recognized in tomato plants that carry the *V2* resistance locus. Environ. Microbiol. 23:1941-1958.

Chen, C., Chen, Y., Jian, H., Yang, D., Dai, Y., Pan, L., Shi, F., Yang, S., and Liu, Q. 2018a. Large-scale identification and characterization of *Heterodera avenae* putative effectors suppressing or inducing cell death in *Nicotiana benthamiana*. Front. Plant. Sci. 8:2062.

Chen, J.-Y., Liu, C., Gui, Y.-J., Si, K.-W., Zhang, D.-D., Wang, J., Short, D. P. G., Huang, J.-Q., Li, N.-Y., Liang, Y., Zhang, W.-Q., Yang, L., Ma, X.-F., Li, T.-G., Zhou, L., Wang, B.-L., Bao, Y.-M., Subbarao, K. V., Zhang, G.-Y., and Dai, X.-F. 2018b. Comparative genomics reveals cotton-specific virulence factors in flexible genomic regions in *Verticillium dahliae* and evidence of horizontal gene transfer from *Fusarium*. New Phytol. 217:756-770.

Chen, M.-M., Jiang, M., Shang, J., Lan, X., Yang, F., Huang, J., Nuss, D. L., and Chen, B. 2011. CYP1, a hypovirus-regulated cyclophilin, is required for virulence in the chestnut blight fungus. Mol. Plant Pathol. 12:239-246.

Chen, S., Songkumarn, P., Venu, R. C., Gowda, M., Bellizzi, M., Hu, J., Liu, W., Ebbole, D., Meyers, B., Mitchell, T., and Wang, G.-L. 2013. Identification and characterization of in planta–expressed secreted effector proteins from *Magnaporthe oryzae* that induce cell death in rice. Mol. Plant-Microbe Interact. 26:191-202.

Cheng, Q., Wang, H., Xu, B., Zhu, S., Hu, L., and Huang, M. 2014. Discovery of a novel small secreted protein family with conserved N-terminal IGY motif in Dikarya fungi. BMC Genom. 15:1151.

Chisholm, S. T., Coaker, G., Day, B., and Staskawicz, B. J. 2006. Host-microbe interactions: Shaping the evolution of the plant immune response. Cell 124:803-814.

Coaker, G., Falick, A., and Staskawicz, B. 2005. Activation of a phytopathogenic bacterial effector protein by a eukaryotic cyclophilin. Science 308:548-550.

Dalio, R. J. D., Herlihy, J., Oliveira, T. S., McDowell, J. M., and Machado, M. 2018. Effector biology in focus: A primer for computational prediction and functional characterization. Mol. Plant-Microbe Interact. 31:22-33.

de Guillen, K., Lorrain, C., Tsan, P., Barthe, P., Petre, B., Saveleva, N., Rouhier, N., Duplessis, S., Padilla, A., and Hecker, A. 2019. Structural genomics applied to the rust fungus *Melampsora larici-populina* reveals two candidate effector proteins adopting cystine knot and NTF2-like protein folds. Sci Rep. 9:18084.

de Jonge, R., Bolton, M. D., and Thomma, B. P. H. J. 2011. How filamentous pathogens co-opt plants: The ins and outs of fungal effectors. Curr. Opin. Plant Biol. 14:400-406.

De Wit, P. J. G. M., Mehrabi, R., Van Den Burg, H. A., and Stergiopoulos, I. 2009. Fungal effector proteins: Past, present and future. Mol. Plant Pathol. 10:735-747.

Dodds, P. N., and Rathjen, J. P. 2010. Plant immunity: Towards an integrated view of plant-pathogen interactions. Nat. Rev. Genet. 11:539-548.

Dong, Y., Li, Y., Zhao, M., Jing, M., Liu, X., Liu, M., Guo, X., Zhang, X., Chen, Y., Liu, Y., Liu, Y., Ye, W., Zhang, H., Wang, Y., Zheng, X., Wang, P., and Zhang, Z. 2015. Global genome and transcriptome analyses of *Magnaporthe oryzae* epidemic isolate 98-06 uncover novel effectors and pathogenicity-related genes, revealing gene gain and lose dynamics in genome evolution. PLoS Pathog. 11:e1004801.

Dos Santos, Á. F., Machado, E. B., Stanosz, G. R., and Smith, D. R. 2010. First report of *Septoria musiva* in poplar in Brazil. Trop. Plant Pathol. 35:052-053.

Dos Santos, K. C. G., Pelletier, G., Séguin, A., Guillemette, F., Hawkes, J., Desgagné-Penix, I., and Germain, H. 2021. Unrelated fungal rust candidate effectors act on overlapping plant functions. Microorganisms 9:996.

Dou, D., Kale, S. D., Wang, X., Jiang, R. H. Y., Bruce, N. A., Arredondo, F. D., Zhang, X., and Tyler, B. M. 2008. RXLR-mediated entry of *Phytophthora sojae* effector *Avr1b* into soybean cells does not require pathogen-encoded machinery. Plant Cell 20:1930-1947.

Dunnell, K. L., Berguson, B., McMahon, B., and LeBoldus, J. M. 2016. Variation in resistance of *Populus nigra* to *Sphaerulina musiva* in the north-central United States. Plant Dis. 100:287-291.

Earley, K. W., Haag, J. R., Pontes, O., Opper, K., Juehne, T., Song, K., and Pikaard, C. S. 2006. Gateway-compatible vectors for plant functional genomics and proteomics. Plant J. 45:616-629.

Ebert, M. K., Rangel, L. I., Spanner, R. E., Taliadoros, D., Wang, X., Friesen, T. L., de Jonge, R., Neubauer, J. D., Secor, G. A., Thomma, B. P. H. J., Stukenbrock, E. H., and Bolton, M. D. 2021. Identification and characterization of *Cercospora beticola* necrosis-inducing effector CbNip1. Mol. Plant Pathol. 22:301-316.

Feau, N., and Bernier, L. 2004. First report of shining willow as a host plant for *Septoria musiva*. Plant Dis. 88:770.

Feau, N., Mottet, M.-J., Périnet, P., Hamelin, R. C., and Bernier, L. 2010. Recent advances related to poplar leaf spot and canker caused by *Septoria musiva*. Can. J. Plant Pathol. 32:122-134.

Figueroa, M., Ortiz, D., and Henningsen, E. C. 2021. Tactics of host manipulation by intracellular effectors from plant pathogenic fungi. Curr. Opin. Plant Biol. 62:102054.

Foster, A. J., Pelletier, G., Tanguay, P., and Séguin, A. 2015. Transcriptome analysis of poplar during leaf spot infection with *Sphaerulina* spp. PLoS One 10:e0138162.

Fouché, S., Plissonneau, C., and Croll, D. 2018. The birth and death of effectors in rapidly evolving filamentous pathogen genomes. Curr. Opin. Microbiol. 46:34-42.

Giraldo, M. C., Dagdas, Y. F., Gupta, Y. K., Mentlak, T. A., Yi, M., Martinez-Rocha, A. L., Saitoh, H., Terauchi, R., Talbot, N. J., and Valent, B. 2013. Two distinct secretion systems facilitate tissue invasion by the rice blast fungus *Magnaporthe oryzae*. Nat. Commun. 4:1996.

Gui, Y.-J., Chen, J.-Y., Zhang, D.-D., Li, N.-Y., Li, T.-G., Zhang, W.-Q., Wang, X.-Y., Short, D. P. G., Li, L., Guo, W., Kong, Z.-Q., Bao, Y.-M., Subbarao, K. V., and Dai, X.-F. 2017. *Verticillium dahliae* manipulates plant immunity by glycoside hydrolase 12 proteins in conjunction with carbohydrate-binding module 1. Environ. Microbiol. 19:1914-1932.

Guo, X., Zhong, D., Xie, W., He, Y., Zheng, Y., Lin, Y., Chen, Z., Han, Y., Tian, D., Liu, W., Wang, F., Wang, Z., and Chen, S. 2019. Functional identification of novel cell death-inducing effector proteins from *Magnaporthe oryza*e. Rice 12:59.

Haas, B. J., Kamoun, S., Zody, M. C., Jiang, R. H., Handsaker, R. E., Cano, L. M., Grabherr, M., Kodira, C. D., Raffaele, S., Torto-Alalibo, T., Bozkurt, T. O., Ah-Fong, A. M. V., Alvarado, L., Anderson, V. L., Armstrong, M. R., Avrova, A., Baxter, L., Beynon, J., Boevink, P. C., Bollmann, S. R., Bos, J. I. B., Bulone, V., Cai, G., Cakir, C., Carrington, J. C., Chawner, M., Conti, L., Costanzo, S., Ewan, R., Fahlgren, N., Fischbach, M. A., Fugelstad, J., Gilroy, E. M., Gnerre, S., Green, P. J., Grenville-Briggs, L. J., Griffith, J., Grünwald, N. J., Horn, K., Horner, N. R., Hu, C.-H., Huitema, E., Jeong, D.-H., Jones, A. M. E., Jones, J. D. G., Jones, R. W., Karlsson, E. K., Kunjeti, S. G., Lamour, K., Liu, Z., Ma, L., Maclean, D., Chibucos, M. C., McDonald, H., McWalters, J., Meijer, H. J. G., Morgan, W., Morris, P. F., Munro, C. A., O'Neill, K., Ospina-Giraldo, M., Pinzón, A., Pritchard, L., Ramsahoye, B., Ren, Q., Restrepo, S., Roy, S., Sadanandom, A., Savidor, A., Schornack, S., Schwartz, D. C., Schumann, U. D., Schwessinger, B., Seyer, L., Sharpe, T., Silvar, C., Song, J., Studholme, D. J., Sykes, S., Thines, M., van de Vondervoort, P. J. I., Phuntumart, V., Wawra, S., Weide, R., Win, J., Young, C., Zhou, S., Fry, W., Meyers, B. C., van West, P., Ristaino, J., Govers, F., Birch, P. R. J., Whisson, S. C., Judelson, H. S., and Nusbaum, C. 2009. Genome sequence and analysis of the Irish potato famine pathogen *Phytophthora infestans*. Nature 461:393-398.

Höfgen, R., and Willmitzer, L. 1988. Storage of competent cells for *Agrobacterium* transformation. Nucleic Acids Res. 16:9877.

Huang, Z., Li, H., Zhou, Y., Bao, Y., Duan, Z., Wang, C., Powell, C. A., Chen, B., Zhang, M., and Yao, W. 2022. Predication of the effector proteins secreted by *Fusarium sacchari* using genomic analysis and heterogenous expression. J. Fungi 8:59.

Jacobs, K. A., Collins-Racie, L. A., Colbert, M., Duckett, M., Golden-Fleet, M., Kelleher, K., Kriz, R., LaVallie, E. R., Merberg, D., Spaulding, V., Stover, J., Williamson, M. J., and McCoy, J. M. 1997. A genetic selection for isolating cDNAs encoding secreted proteins. Gene 198: 289-296.

Jaswal, R., Kiran, K., Rajarammohan, S., Dubey, H., Singh, P. K., Sharma, Y., Deshmukh, R., Sonah, H., Gupta, N., and Sharma, T. R. 2020. Effector biology of biotrophic plant fungal pathogens: Current advances and future prospects. Microbiol. Res. 241:126567.

Jeger, M., Bragard, C., Caffier, D., Candresse, T., Chatzivassiliou, E., Dehnen-Schmutz, K., Gilioli, G., Grégoire, J.-C., Jaques Miret, J. A., Macleod, A., Navarro, M. N., Niere, B., Parnell, S., Potting, R., Rafoss, T., Rossi, V., Urek, G., Van Bruggen, A., Van Der Werf, W., West, J., Winter, S., Boberg, J., Gonthier, P., and Pautasso, M. 2018. Pest categorisation of *Sphaerulina musiva*. EFSA J. 16:e05247.

Jones, J. D. G., and Dangl, J. L. 2006. The plant immune system. Nature 444:323-329.

Kamoun, S., Lindqvist, H., and Govers, F. 1997. A novel class of elicitin-like genes from *Phytophthora infestans*. Mol. Plant-Microbe Interact. 10:1028-1030.

Keppler, L. D., Baker, C. J., and Atkinson, M. M. 1989. Active oxygen production during a bacteria-induced hypersensitive reaction in tobacco suspension cells. Phytopathology 79:974-978.

Kim, D., Pertea, G., Trapnell, C., Pimentel, H., Kelley, R., and Salzberg, S. L. 2013. TopHat2: Accurate alignment of transcriptomes in the presence of insertions, deletions and gene fusions. Genome Biol. 14:R36.

Kong, G., Zhao, Y., Jing, M., Huang, J., Yang, J., Xia, Y., Kong, L., Ye, W., Xiong, Q., Qiao, Y., Dong, S., Ma, W., and Wang, Y. 2015. The activation of *Phytophthora* effector Avr3b by plant cyclophilin is required for the Nudix hydrolase activity of Avr3b. PLoS Pathog. 11:e1005139.

Krogh, A., Larsson, B., von Heijne, G., and Sonnhammer, E. L. 2001. Predicting transmembrane protein topology with a hidden Markov model: Application to complete genomes. J. Mol. Biol. 305:567-580.

Krombach, S., Reissmann, S., Kreibich, S., Bochen, F., and Kahmann, R. 2018. Virulence function of the *Ustilago maydis* sterol carrier protein 2. New Phytol. 220:553-566.

Lai, M.-W., and Liou, R.-F. 2018. Two genes encoding GH10 xylanases are essential for the virulence of the oomycete plant pathogen *Phytophthora parasitica*. Curr. Genet. 64:931-943.

Lam, E., Kato, N., and Lawton, M. 2001. Programmed cell death, mitochondria and the plant hypersensitive response. Nature 411:848-853.

Lenz, R. R., Louie, K. B., Søndreli, K. L., Galanie, S. S., Chen, J.-G., Muchero, W., Bowen, B. P., Northen, T. R., and LeBoldus, J. M. 2021. Metabolomic patterns of Septoria canker resistant and susceptible *Populus trichocarpa* genotypes 24 hours postinoculation. Phytopathology 111:2052-2066.

Li, F., Yuan, G., Liao, T., Li, Q., and Lin, W. 2017. Leaf spot of tobacco caused by *Fusarium proliferatum*. J. Gen. Plant Pathol. 83:264-267.

Li, Z., Wang, Y., Fan, Y., Ahmad, B., Wang, X., Zhang, S., Zhu, Y., Gao, L., Chang, P., and Wang, X. 2021. Transcriptome analysis of the grape-*Elsinoë ampelina* pathosystem reveals novel effectors and a robust defense response. Mol. Plant-Microbe Interact. 34:110-121.

Liang, H., Staton, M., Xu, Y., Xu, T., and LeBoldus, J. 2014. Comparative expression analysis of resistant and susceptible *Populus* clones inoculated with *Septoria musiva*. Plant Sci. 223:69-78.

Liu, T., Song, T., Zhang, X., Yuan, H., Su, L., Li, W., Xu, J., Liu, S., Chen, L., Chen, T., Zhang, M., Gu, L., Zhang, B., and Dou, D. 2014. Unconventionally secreted effectors of two filamentous pathogens target plant salicylate biosynthesis. Nat. Commun. 5:4686.

Livak, K. J., and Schmittgen, T. D. 2001. Analysis of relative gene expression data using real-time quantitative PCR and the $2^{-\Delta\Delta C_T}$ method. Methods 25:402-408.

Lo Presti, L., Lanver, D., Schweizer, G., Tanaka, S., Liang, L., Tollot, M., Zuccaro, A., Reissmann, S., and Kahmann, R. 2015. Fungal effectors and plant susceptibility. Annu. Rev. Plant Biol. 66:513-545.

López-Solanilla, E., Bronstein, P. A., Schneider, A. R., and Collmer, A. 2004. HopPtoN is a *Pseudomonas syringae* Hrp (type III secretion system) cysteine protease effector that suppresses pathogen-induced necrosis associated with both compatible and incompatible plant interactions. Mol. Microbiol. 54:353-365.

Lorrain, C., Hecker, A., and Duplessis, S. 2015. Effector-mining in the poplar rust fungus *Melampsora larici-populina* secretome. Front. Plant Sci. 6:1051.

Ma, C., Duan, C., Jiang, Y., Nagle, M., Peremyslova, E., Goddard, A., and Strauss, S. H. 2022a. Factors affecting *in vitro* regeneration in the model tree *Populus trichocarpa*: II. Heritability estimates, correlations among explant types, and genetic interactions with treatments among wild genotypes. In Vitro Cell. Dev. Biol. Plant 58:853-864.

Ma, C., Goddard, A., Peremyslova, E., Duan, C., Jiang, Y., Nagle, M., and Strauss, S. H. 2022b. Factors affecting *in vitro* regeneration in the model tree *Populus trichocarpa*: I. Medium, environment, and hormone controls on organogenesis. In Vitro Cell. Dev. Biol. Plant 58:837-852.

Ma, Z., Song, T., Zhu, L., Ye, W., Wang, Y., Shao, Y., Dong, S., Zhang, Z., Dou, D., Zheng, X., Tyler, B. M., and Wang, Y. 2015. A *Phytophthora sojae* glycoside hydrolase 12 protein is a major virulence factor during soybean infection and is recognized as a PAMP. Plant Cell 27:2057-2072.

Ma, Z., Zhu, L., Song, T., Wang, Y., Zhang, Q., Xia, Y., Qiu, M., Lin, Y., Li, H., Kong, L., Fang, Y., Ye, W., Wang, Y., Dong, S., Zheng, X., Tyler, B. M., and Wang, Y. 2017. A paralogous decoy protects *Phytophthora sojae* apoplastic effector PsXEG1 from a host inhibitor. Science 355: 710-714.

Meng, Q.-L., Tang, D.-J., Fan, Y.-Y., Li, Z.-J., Zhang, H., He, Y.-Q., Jiang, B.-L., and Lu, G.-T., and Tang, J.-L. 2011. Effect of interactions between Mip and PrtA on the full extracellular protease activity of *Xanthomonas campestris* pathovar *campestris*. FEMS Microbiol. Lett. 323: 180-187.

Muchero, W., Sondreli, K. L., Chen, J.-G., Urbanowicz, B. R., Zhang, J., Singan, V., Yang, Y., Brueggeman, R. S., Franco-Coronado, J., Abraham, N., Yan, J.-Y., Moremen, K. W., Weisberg, A. J., Chang, J. H., Lindquist, E., Barry, K., Ranjan, P., Jawdy, S., Schmutz, J., Tuskan, G. A., and LeBoldus, J. M. 2018. Association mapping, transcriptomics, and transient expression identify candidate genes mediating plant-pathogen interactions in a tree. Proc. Natl. Acad. Sci. U.S.A. 115:11573-11578.

Nguyen, H. P., Chakravarthy, S., Velásquez, A. C., McLane, H. L., Zeng, L., Nakayashiki, H., Park, D.-H., Collmer, A., and Martin, G. B. 2010. Methods to study PAMP-triggered immunity using tomato and *Nicotiana benthamiana*. Mol. Plant-Microbe Interact. 23:991-999.

Niemczyk, M., and Thomas, B. R. 2020. Growth parameters and resistance to *Sphaerulina musiva*-induced canker are more important than wood density for increasing genetic gain from selection of *Populus* spp. hybrids for northern climates. Ann. For. Sci. 77:26.

Ökmen, B., Mathow, D., Hof, A., Lahrmann, U., Aßmann, D., and Doehlemann, G. 2018. Mining the effector repertoire of the biotrophic fungal pathogen *Ustilago hordei* during host and non-host infection. Mol. Plant Pathol. 19:2603-2622.

Oltval, Z. N., Milliman, C. L., and Korsmeyer, S. J. 1993. Bcl-2 heterodimerizes in vivo with a conserved homolog, Bax, that accelerates programed cell death. Cell 74:609-619.

Ostry, M. E., and McNabb, H. S., Jr. 1985. Susceptibility of *Populus* species and hybrids to disease in the north central United States. Plant Dis. 69:755-757.

Ostry, M. E., Wilson, L. F., and McNabb, H. S., Jr. 1989. Impact and Control of Septoria musiva on Hybrid Poplars (General Technical Report NC-133). U.S. Dept. of Agriculture, Forest Service, North Central Forest Experiment Station, St. Paul, MN.

Polle, A., Janz, D., Teichmann, T., and Lipka, V. 2013. Poplar genetic engineering: Promoting desirable wood characteristics and pest resistance. Appl. Microbiol. Biotechnol. 97:5669-5679.

Qian, Y., Zheng, X., Wang, X., Yang, J., Zheng, X., Zeng, Q., Li, J., Zhuge, Q., and Xiong, Q. 2022. Systematic identification and functional characterization of the CFEM proteins in poplar fungus *Marssonina brunnea*. Front. Cell. Infect. Microbiol. 12:1045615.

Rafiei, V., Vélëz, H., and Tzelepis, G. 2021. The role of glycoside hydrolases in phytopathogenic fungi and oomycetes virulence. Int. J. Mol. Sci. 22:9359.

Rahman, M. S., Madina, M. H., Plourde, M. B., Dos Santos, K. C. G., Huang, X., Zhang, Y., Laliberté, J.-F., and Germain, H. 2021. The fungal effector Mlp37347 alters plasmodesmata fluxes and enhances susceptibility to pathogen. Microorganisms 9:1232.

Reindl, M., Hänsch, S., Weidtkamp-Peters, S., and Schipper, K. 2019. A potential lock-type mechanism for unconventional secretion in fungi. Int. J. Mol. Sci. 20:460.

Ridout, C. J., Skamnioti, P., Porritt, O., Sacristan, S., Jones, J. D. G., and Brown, J. K. M. 2006. Multiple avirulence paralogues in cereal powdery mildew fungi may contribute to parasite fitness and defeat of plant resistance. Plant Cell 18:2402-2414.

Rocafort, M., Fudal, I., and Mesarich, C. H. 2020. Apoplastic effector proteins of plant-associated fungi and oomycetes. Curr. Opin. Plant Biol. 56:9-19.

Sánchez-Vallet, A., Fouché, S., Fudal, I., Hartmann, F. E., Soyer, J. L., Tellier, A., and Croll, D. 2018. The genome biology of effector gene evolution in filamentous plant pathogens. Annu. Rev. Phytopathol. 56:21-40.

Sannigrahi, P., Ragauskas, A. J., and Tuskan, G. A. 2010. Poplar as a feedstock for biofuels: A review of compositional characteristics. Biofuel Bioprod. Biorefin. 4:209-226.

Selin, C., de Kievit, T. R., Belmonte, M. F., and Fernando, W. G. D. 2016. Elucidating the role of effectors in plant-fungal interactions: Progress and challenges. Front. Microbiol. 7:600.

Søndreli, K. L., Keriö, S., Frost, K., Muchero, W., Chen, J.-G., Haiby, K., Gantz, C., Tuskan, G., and LeBoldus, J. M. 2020. Outbreak of Septoria canker caused by *Sphaerulina musiva* on *Populus trichocarpa* in eastern Oregon. Plant Dis. 104:3266-3266.

Sperschneider, J., Dodds, P. N., Gardiner, D. M., Manners, J. M., Singh, K. B., and Taylor, J. M. 2015. Advances and challenges in computational prediction of effectors from plant pathogenic fungi. PLoS Pathog. 11:e1004806.

Stael, S., Kmiecik, P., Willems, P., Van Der Kelen, K., Coll, N. S., Teige, M., and Van Breusegem, F. 2015. Plant innate immunity–sunny side up? Trends Plant Sci. 20:3-11.

Stergiopoulos, I., and de Wit, P. J. G. M. 2009. Fungal effector proteins. Annu. Rev. Phytopathol. 47:233-263.

Strauss, S. H., Slavov, G. T., and DiFazio, S. P. 2022. Gene-editing for production traits in forest trees: Challenges to integration and gene target identification. Forests 13:1887.

Sun, J., Sun, C.-H., Chang, H.-W., Yang, S., Liu, Y., Zhang, M.-Z., Hou, J., Zhang, H., Li, G.-H., and Qin, Q.-M. 2021. Cyclophilin BcCyp2 regulates infection-related development to facilitate virulence of the gray mold fungus *Botrytis cinerea*. Int. J. Mol. Sci. 22:1694.

Sun, Y., Wang, Y., Zhang, X., Chen, Z., Xia, Y., Wang, L., Sun, Y., Zhang, M., Xiao, Y., Han, Z., Wang, Y., and Chai, J. 2022. Plant receptor-like protein activation by a microbial glycoside hydrolase. Nature 610:335-342.

Tabima, J. F., Søndreli, K. L., Keriö, S., Feau, N., Sakalidis, M. L., Hamelin, R. C., and LeBoldus, J. M. 2020. Population genomic analyses reveal connectivity via human-mediated transport across *Populus* plantations in North America and an undescribed subpopulation of *Sphaerulina musiva*. Mol. Plant-Microbe Interact. 33:189-199.

Terauchi, R., and Yoshida, K. 2010. Towards population genomics of effector–effector target interactions. New Phytol. 187:929-939.

Ünal, C. M., and Steinert, M. 2015. FKBPs in bacterial infections. Biochim. Biophys. Acta 1850:2096-2102.

Viaud, M., Brunet-Simon, A., Brygoo, Y., Pradier, J.-M., and Levis, C. 2003. Cyclophilin A and calcineurin functions investigated by gene inactivation, cyclosporin A inhibition and cDNA arrays approaches in the phytopathogenic fungus *Botrytis cinerea*. Mol. Microbiol. 50: 1451-1465.

Viaud, M. C., Balhadère, P. V., and Talbot, N. J. 2002. A *Magnaporthe grisea* cyclophilin acts as a virulence determinant during plant infection. Plant Cell 14:917-930.

Wang, P., Cardenas, M. E., Cox, G. M., Perfect, J. R., and Heitman, J. 2001. Two cyclophilin A homologs with shared and distinct functions important for growth and virulence of *Cryptococcus neoformans*. EMBO Rep. 2:511-518.

Wang, Q., Han, C., Ferreira, A. O., Yu, X., Ye, W., Tripathy, S., Kale, S. D., Gu, B., Sheng, Y., Sui, Y., Wang, X., Zhang, Z., Cheng, B., Dong, S., Shan, W., Zheng, X., Dou, D., Tyler, B. M., and Wang, Y. 2011. Transcriptional programming and functional interactions within the *Phytophthora sojae* RXLR effector repertoire. Plant Cell 23:2064-2086.

Wang, Y., Tyler, B. M., and Wang, Y. 2019. Defense and counterdefense during plant-pathogenic oomycete infection. Annu. Rev. Microbiol. 73:667-696.

Yang, B., Wang, Q., Jing, M., Guo, B., Wu, J., Wang, H., Wang, Y., Lin, L., Wang, Y., Ye, W., Dong, S., and Wang, Y. 2017. Distinct regions of the *Phytophthora* essential effector Avh238 determine its function in cell death activation and plant immunity suppression. New Phytol. 214: 361-375.

Yin, W., Wang, Y., Chen, T., Lin, Y., and Luo, C. 2018. Functional evaluation of the signal peptides of secreted proteins. Bio-protocol 8:e2839.

Yin, Z., Wang, N., Duan, W., Pi, L., Shen, D., and Dou, D. 2021. *Phytophthora capsici* CBM1-containing protein CBP3 is an apoplastic effector with plant immunity-inducing activity. Mol. Plant Pathol. 22:1358-1369.

Zhang, C.-J., Wang, S.-X., Liang, Y.-N., Wen, S.-H., Dong, B.-Z., Ding, Z., Guo, L.-Y., and Zhu, X.-Q. 2021a. Candidate effectors from *Botryosphaeria dothidea* suppress plant immunity and contribute to virulence. Int. J. Mol. Sci. 22:552.

Zhang, L., Yan, J., Fu, Z., Shi, W., Ninkuu, V., Li, G., Yang, X., and Zeng, H. 2021b. FoEG1, a secreted glycoside hydrolase family 12 protein from *Fusarium oxysporum*, triggers cell death and modulates plant immunity. Mol. Plant Pathol. 22:522-538.

Zhang, M., Xie, S., Zhao, Y., Meng, X., Song, L., Feng, H., and Huang, L. 2019. Hce2 domain-containing effectors contribute to the full virulence of *Valsa mali* in a redundant manner. Mol. Plant Pathol. 20:843-856.

Zhang, Y., Wei, J., Qi, Y., Li, J., Amin, R., Yang, W., and Liu, D. 2020. Predicating the effector proteins secreted by *Puccinia triticina* through transcriptomic analysis and multiple prediction approaches. Front. Microbiol. 11:538032.

Zhang, Y., Zhang, K., Fang, A., Han, Y., Yang, J., Xue, M., Bao, J., Hu, D., Zhou, B., Sun, X., Li, S., Wen, M., Yao, N., Ma, L.-J., Liu, Y., Zhang, M., Huang, F., Luo, C., Zhou, L., Li, J., Chen, Z., Miao, J., Wang, S., Lai, J., Xu, J.-R., Hsiang, T., Peng, Y.-L., and Sun, W. 2014. Specific adaptation of *Ustilaginoidea virens* in occupying host florets revealed by comparative and functional genomics. Nat. Commun. 5: 3849.

Zhou, Y., Keyhani, N. O., Zhang, Y., Luo, Z., Fan, Y., Li, Y., Zhou, Q., Chen, J., and Pei, Y. 2016. Dissection of the contributions of cyclophilin genes to development and virulence in a fungal insect pathogen. Environ. Microbiol. 18:3812-3826.

Zhu, W., Ronen, M., Gur, Y., Minz-Dub, A., Masrati, G., Ben-Tal, N., Savidor, A., Sharon, I., Eizner, E., Valerius, O., Braus, G. H., Bowler, K., Bar-Peled, M., and Sharon, A. 2017. BcXYG1, a secreted xyloglucanase from *Botrytis cinerea*, triggers both cell death and plant immune responses. Plant Physiol. 175:438-456.